Developed quantum turbulence and its decay

Cite as: Phys. Fluids **24**, 011301 (2012); https://doi.org/10.1063/1.3678335
Submitted: 21 November 2011 • Accepted: 14 December 2011 • Published Online: 31 January 2012

L. Skrbek and K. R. Sreenivasan

Developed quantum turbulence and its decay[a)]

L. Skrbek[1] and K. R. Sreenivasan[2,b)]
[1]*Faculty of Mathematics and Physics, Charles University, Ke Karlovu 3, 12116 Prague 2, Czech Republic*
[2]*Department of Physics and Courant Institute of Mathematical Sciences, New York University, New York 10012, USA*

(Received 21 November 2011; accepted 14 December 2011; published online 31 January 2012)

This article is primarily a review of our knowledge of the correspondence between classical and quantum turbulence, though it is interspersed with a few new interpretations. This review is deemed timely because recent work in quantum turbulence promises to provide a better understanding of aspects of classical turbulence, though the two fields of turbulence have similarities as well as differences. We pay a particular attention to the conceptually simplest case of zero temperature limit where quantum turbulence consists of a tangle of quantized vortex line and represents a simple prototype of turbulence. At finite temperature, we anchor ourselves at the level of two-fluid description of the superfluid state—consisting of a normal viscous fluid and a frictionless superfluid—and review much of the available knowledge on quantum turbulence in liquid helium (both He II and ^{3}He-B). We consider counterflows in which the normal and superfluid components flow against each other, as well as co-flows in which the direction of the two fluids is the same. We discuss experimental methods, phenomenological results as well as key theoretical concepts. © *2012 American Institute of Physics*. [doi:10.1063/1.3678335]

I. INTRODUCTION

The subject of this review is quantum turbulence (QT).[1] QT can be defined loosely as the most general dynamical motion of tangles of thin quantized vortex lines with certain special properties to be described subsequently. It appears from recent research that QT may help us acquire a deeper understanding of classical turbulence in viscous fluids. Accordingly, our particular focus here is the connection between QT and classical turbulence. Although QT differs from its classical counterpart in some important ways, many of its properties can be understood in terms of the existing phenomenology of classical turbulence. QT is also an interesting subject in its own right: it provides a formidable intellectual challenge and represents today one of the most lively parts of research in low temperature physics. We thus include considerable discussion of the observations on QT.

QT occurs in quantum fluids. Quantum fluids are so called because some of their properties—which we discuss at some length below—depend on quantum physics. While quantum turbulence may occur in a number of circumstances such as the interior of neutron stars and various Bose-Einstein condensates, we restrict attention to two traditional quantum fluids. They are the non-radioactive isotopes of liquid helium: the superfluid phase of ^{4}He and the so-called superfluid B phase of ^{3}He. The left superscript 4 in the former refers to the fact that the nucleus of the atom contains two protons and two neutrons; the superscript 3 in the latter refers to the lighter isotope consisting of two protons and one neutron. The two protons and two neutrons of ^{4}He, together with two electrons which make the s-orbital fully populated, constitute a spherically symmetric atom with zero spin and represents a boson. On the other hand, since ^{3}He has only one neutron in

[a)]This review is an expanded version of the invited talk given by KRS at the Division of Fluid Dynamics meeting of the American Physical Society in November 2007. A short version will appear in "Ten Chapters in Turbulence" to be published by Cambridge University Press.
[b)]Electronic mail: skrbek@fzu.cz, krs3@nyu.edu.

its nucleus, the atom possesses a spin of 1/2 and represents a fermion. At normal pressure, ^{4}He and ^{3}He liquify at 4.2 K and 3.2 K, respectively. By liquifying ^{4}He more than a century ago, H. Kamerlingh-Onnes in Leiden established the foundations of low temperature physics.

The differences in the atomic structure of ^{4}He and ^{3}He do not lead to any appreciable differences in collective behavior at room temperature, and both behave nearly as ideal gases. At low temperatures, however, the physical properties of ^{4}He and ^{3}He are very different, being governed by Bose-Einstein and Fermi-Dirac quantum statistics, respectively. Together, these two substances have served the cryogenic fluid dynamics community as working fluids with well-known physical properties. Indeed, our current level of understanding of QT comes almost exclusively from the study of these two liquids. ^{4}He, which is by far the more abundant isotope, undergoes a phase transition below about 2.17 K. This new phase is known historically as helium II, or simply as He II. ^{3}He acquires superfluid properties only below about 1 mK.

The phenomenological description of He II as well as ^{3}He-B involves two fluids and in frame of this so-called two-fluid model they are described as consisting of a viscous normal fluid that coexists with an inviscid superfluid. In the absence of quantized vortices (see below), under isothermal conditions these two fluids support two independent velocity fields simultaneously, and the superfluid component can flow without dissipation while being subject to certain quantum mechanical constraints. These quantum restrictions are that the only form of rotational motion allowed in the superfluid component is a thin vortex line, whose circulation around its core is not arbitrary as in classical fluids, but quantized in units $\kappa = 2\pi\hbar/m$; here $\hbar$ is the Planck's constant and m is the mass of a superfluid particle (such as the ^{4}He atom or a Cooper pair of two ^{3}He atoms). As we shall see later, the presence of quantized vortices couples the superfluid and normal velocity fields by the action of the so-called mutual friction force. In liquid ^{4}He at 2.17 K, nearly all the fluid is normal but it becomes mostly superfluid as one approaches 0 K. Similar considerations apply to ^{3}He, however, at much lower temperature around and below 1 mK.

Frictionless flow and quantization of circulation have quantum mechanical origins and lie outside the common experience with classical fluids. The subject of superfluids has thus generally been relegated to the backwaters of mainstream fluid dynamics. The focus of low-temperature physicists has been the microscopic structure of superfluids, which does not naturally invite the attention of experts on classical fluids. However, perhaps amazingly, in some circumstances there exists a state of superfluid flow that is similar to classical turbulence, qualitatively and quantitatively, in which superfluids are endowed with quasiclassical properties such as effective friction and finite heat conductivity.[2–4] This is QT, also known often as superfluid turbulence. Historically, this kind of turbulence in He II was mentioned as a theoretical possibility by Feynman,[2] who was the first to recognize that QT ought to take the form of a random tangle of quantized vortices.

Studies of QT in He II started more than fifty years ago by Vinen,[5] with pioneering experiments on thermally induced counterflow in which the normal and superfluid components move in opposite directions. This counterflow has no direct classical counterpart. For this reason, quantum fluids were thought to be different in character from classical fluids. The result was an almost disconnected development of the fields of hydrodynamic and quantum turbulence. Vinen[5] also developed a phenomenological description of counterflow turbulence. By 1980s, in fact, a fair level of understanding of counterflow QT was achieved, and experiments on thermal counterflow essentially came to a natural halt. In the nineties, however, interest in QT was revived, in view of the experiments where He II turbulence was generated classically (between counterrotating discs[6] and by a towed grid[7,8]). It was soon realized that, owing to the coupling by the mutual friction force of large-scale normal and superfluid eddies, the classical and QT fields (despite the quantum mechanical restrictions mentioned above) bear important similarities.[9]

The rest of the article is organized as follows. Section II provides a phenomenological background on quantum fluids that is required to follow the developments in QT. Readers familiar with these topics can skip this section. Section III discusses counterflow in He II while the important case of decaying counterflow turbulence is considered in Sec. IV. The co-flow case of QT in He II above about 1 K, which has contributed to the rejuvenation of interest in QT, is the subject of Sec. V. Below about 1 K, He II is essentially a pure superfluid. A summary of results obtained at these temperatures of He II is the subject of Sec. VI, which also includes results for ^{3}He-B at low enough temperatures for it to be in essentially the pure superfluid state. QT in stationary

normal fluid of ^{3}He-B is the subject of Sec. VII. Section VIII attempts a cogent discussion of the results at the empirical level while and Sec. IX represents a similar attempt at a somewhat more formal level. The paper ends with a summary of conclusions in Sec. X.

II. BASIC BACKGROUND

A. Phase diagrams of ^{4}He and ^{3}He

Figure 1 shows the low temperature parts of equilibrium pressure-temperature phase diagrams for both isotopes of helium. The most striking feature is the absence of triple point. In order to solidify them, external pressures of the order of 30 bar must be applied. One can interpret this fact in terms of melting at ambient pressure due to zero point motion, which is a quantum mechanical effect. Zero-point energy is the lowest possible energy that a quantum mechanical system may have in the ground state. In contrast, all motion in classical systems ceases at 0 K.

Normal liquid ^{4}He phase, historically called He I, represents a classical viscous Navier-Stokes fluid possessing a kinematic viscosity that is on the order of 10^{-4} cm^2/s, depending slightly on temperature and pressure.[10] Together with the cold ^{4}He gas (whose flow properties can experimentally be tuned easily by changing temperature and pressure), He I serves as very useful classical viscous working fluid, offering a serious medium for classical fluid dynamics with continuously tuneable properties (over at least two orders of magnitude of kinematic viscosity)

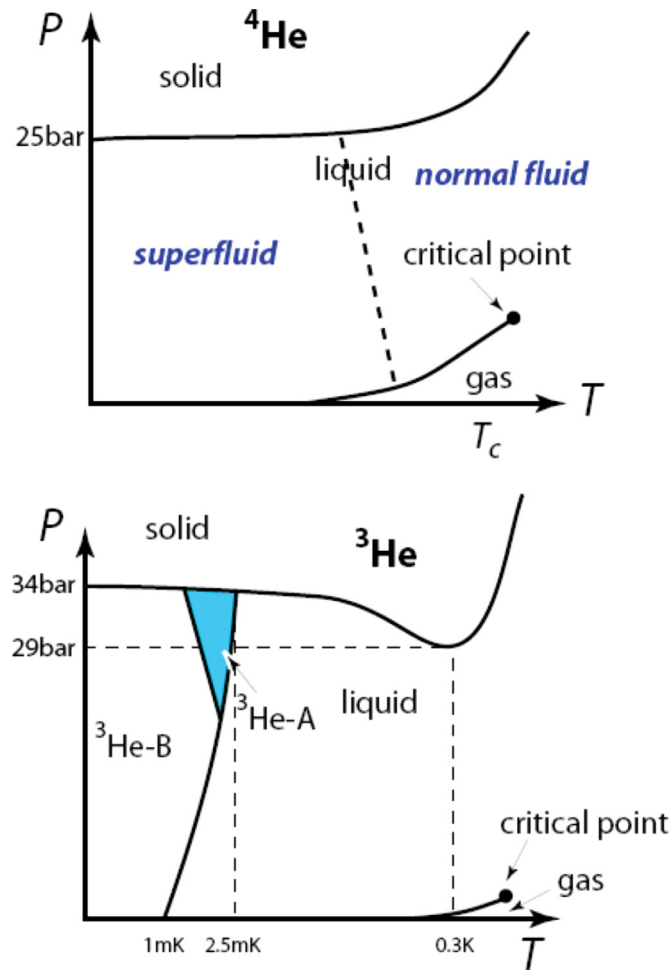

FIG. 1. (Color online) Phase diagrams of the two isotopes of helium. Note that there is no triple point and both isotopes stay in a superfluid liquid phase down to absolute zero (except at high pressures). The region to the left of the dashed line in the upper figure is He II. ^{3}He is a magnetic liquid and its state depends on the externally applied magnetic field (see text for details).

suitable for generating flows not only with high Reynolds and Rayleigh numbers but also large ranges of these flow parameters.[11] This subject has now assumed its own life and is often called cryogenic fluid dynamics; see Donnelly and Sreenivasan,[12] Skrbek, Niemela, and Donnelly,[13] and Niemela and Sreenivasan.[14]

B. Superfluid phase of ^{4}He-He II

As already noted, if the temperature of normal liquid He I is lowered along the saturated vapor curve, ^{4}He reaches its superfluid state, He II, at about $T_\lambda \cong 2.17$ K (see Figure 1); see dashed line. The physical reason for superfluidity is the bosonic character of ^{4}He atoms that in 3d momentum space can undergo quantum mechanical Bose condensation. For deeper discussion of underlying physics of superfluidity, we direct the reader to one of many textbooks, such as Ref. 15; here, we shall limit ourselves with the two-fluid phenomenological description proposed by Landau (see, e.g., Refs. 15 and 16), which is sufficient to discuss QT.

Briefly, superfluidity can be understood as the manifestation of quantum mechanics at the macroscopic scale. Particles such as protons or electrons are quantum-mechanically described by means of the wave function Ψ, its squared amplitude giving us the probability of finding the particle in a particular space. For superfluidity, the superfluid in the entire sample must be described by a single, macroscopic, wave function of the form $\Psi = \sqrt{\rho_s}\exp\{i\phi\}$, where ϕ denotes the macroscopic phase. The square of the wave function amplitude, i.e., the probability of finding the superfluid liquid in space, can qualitatively be thought of as the superfluid density ρ_s. For deeper discussion of this topic, see, e.g., Ref. 15.

By applying the impulse operator, $-i\hbar\nabla$, to the macroscopic wave function and expressing the impulse per helium atom of mass m_{He} as $\boldsymbol{p} = m_{He}\boldsymbol{v}_s$, one sees that the superfluid velocity is given by the spatial gradient of the macroscopic phase, $\boldsymbol{v}_s \propto \nabla\phi$. From here, it immediately follows that the superfluid velocity field must be irrotational: curl $\boldsymbol{v}_s = 0$. Assuming incompressible flow, i.e., div $\boldsymbol{v}_s = 0$, one sees a striking and deep similarity between superfluidity and electromagnetism. Maxwell's equations *in vacuo* for magnetic induction $\boldsymbol{B}$ are of the same form exactly: div $\boldsymbol{B} = 0$; curl $\boldsymbol{B} = 0$. This analogy will be used later while calculating the superfluid velocity field from the Biot-Savart law in the presence of quantized vortices in the flow.

With good accuracy, He II behaves as an intimate mixture of two co-penetrating but non-interacting fluid components: the viscous normal fluid (of density ρ_n and velocity $\boldsymbol{v}_n$) and the inviscid superfluid (of density ρ_s and velocity $\boldsymbol{v}_s$), where $\rho = \rho_n + \rho_s$ is the total density of liquid helium. At T_λ, He II is entirely normal; the ratio ρ_n/ρ_s falls with decreasing temperature, until in the $T \to 0$ limit He II is entirely superfluid (Figure 2). The ρ_n/ρ_s ratio was first experimentally established in the Andronikashivili[17] experiment with a pile of thin closely spaced discs arranged as a torsional pendulum (see the inset in Figure 2) hanging in He II on a thin torsional fibre. If the discs are suspended in a classical viscous fluid of finite kinematic viscosity ν and the vertical distance between them is much less than the penetration depth $\delta = 2\nu/\Omega$, where Ω is the angular frequency of torsional oscillations, the fluid is firmly trapped between the discs and contributes to the moment of inertia $\boldsymbol{J}$ of the pendulum. This is the case of He I. As the temperature is lowered below T_λ, the period of oscillations increases, as the superfluid, being inviscid, stays at rest and does not contribute to $\boldsymbol{J}$. As the total density of He II stays approximately constant, it follows that the relative content of superfluid with lowering temperature increases in the fashion shown in Figure 2. We discuss below, however, that on exceeding critical velocity somewhere in the flow this physical picture becomes altered, as quantized vortices appear in the flow.

At temperatures above about 1 K the dynamic viscosity of the normal fluid is rather small and similar in magnitude to that of He I. At lower temperatures, however, the viscosity rises sharply, as the mean free path of the gas of excitations (which is, in fact, the normal fluid) increases, gradually becoming of the order of the size of the container (or any macroscopic scale of interest) and classical hydrodynamic description for the normal fluid is no longer justified. Instead, individual scattering evens of quasiparticles, the so-called phonons and rotons, ought to be considered.

Based on the form of the dispersion relation in He II, Landau predicted that superfluidity in He II will disappear at flow velocities exceeding a critical value of about 60 m/s (due to the emission of quasiparticles called rotons). In a more general sense, the Landau criterion applies for any

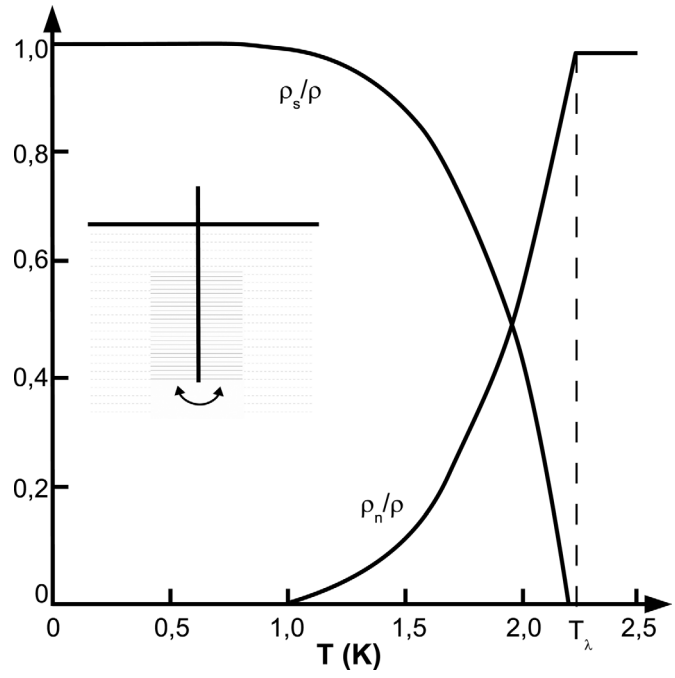

FIG. 2. Temperature dependence of the normal and superfluid density ratio in He II. The inset shows the principle of the Andronikashvili torsional pendulum experiment leading to this measured dependence.

superfluid: on exceeding certain critical velocity, it becomes energetically favorable to generate quasiparticles, which means the onset of dissipation from the point of standard fluid dynamics.

C. Quantization of circulation and quantized vortices in He II

The idea of quantized circulation belongs to Onsager[18] and was further developed by Feynman.[2] The most convenient way to introduce quantized vortices follows from the definition of macroscopic wave function in a superfluid. From its functional form $\Psi = \sqrt{\rho_s}\exp\{i\phi\}$, it follows that Ψ remains constant if the macroscopic phase ϕ changes by $\pm 2\pi n$, where n is an integer.

The circulation Γ is defined as an integral along closed path L inside the superfluid,

$$\Gamma = \oint_L \boldsymbol{v}_s d\ell = \frac{\hbar}{m_4}\oint_L \nabla\phi d\ell, \tag{1}$$

and does not depend on the path itself, as long as it remains inside the liquid.

Imagine an axis (Figure 3(a)) that crosses at some interior point O a singly connected area encircled by the loop L. The value of the wave function must remain constant in looping round L. This condition is satisfied even if the phase changes by $\pm 2\pi n$ by going round the loop. However,

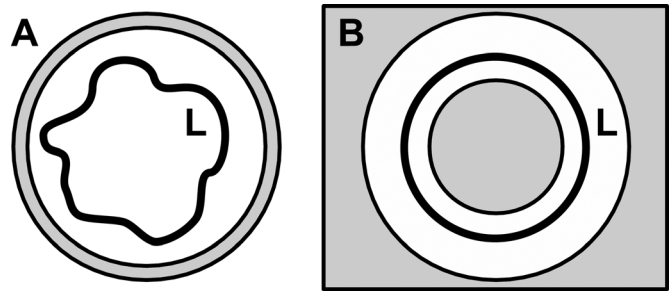

FIG. 3. Simply and multiply connected regions in superfluid helium. The shaded regions lie outside the fluid. The point O lies somewhere inside the loop in A, and inside the shaded circle in B.

by shrinking the loop closer and closer to the point O, we arrive at a singularity, except if $n = 0$ or $\Gamma = 0$.

For multiply connected regions (Figure 3(b)) the situation is different, as the loop cannot be shrunk to the point O chosen within the loop L but inside the wall, i.e., outside the superfluid liquid. One can be consistent only if the circulation becomes quantized as

$$\Gamma = n\frac{h}{m_4} = n\kappa, \tag{2}$$

where $\kappa = 9{,}997 \times 10^{-8}$ m^2/s is the quantum of circulation. An alternative point of view[16,18,19] is that the angular momentum per one helium atom is quantized in units of $\hbar$.

Transformation from singly to multiply connected regions in He II could occur spontaneously. One can imagine that the superfluid becomes threaded by Angström size "holes"—cores of quantized vortices—and circulates round them; see Fig. 4. Vorticity is therefore restricted to cores and is zero elsewhere. In case of one straight singly quantized vortex, the velocity of superfluid component is $v_s = \hbar n/(m_4 r) = \kappa n/(2\pi r)$, where r denotes the radial distance from the axis. The atomic size of the core is of order of so-called healing length ξ, which represents a characteristic distance over which the amplitude of the macroscopic wave function changes. As illustrated in Fig. 4, the superfluid density is zero on the axis but rises rapidly with distance towards its bulk value, $\rho_{s.}$

A simple argument will show that in He II it is energetically favorable if quantized vortices are singly quantized (i.e., $n = 1$). The energy of the unit length of vortex, i.e., the kinetic energy of the circulating superfluid is

$$\varepsilon_v = \int_{a_0}^{b} \pi \rho_s v_s^2 r dr = \frac{n^2 \rho_s \kappa^2}{4\pi} \ln\left(\frac{b}{a_0}\right), \tag{3}$$

where a_0 is the radius of the core and b denotes either the size of the vessel or characteristic distance between quantized vortices. As $\varepsilon_v \propto n^2$, it is energetically favorable that an n-fold quantized vortex splits into n singly quantized vortices.

For quantized vortices the Kelvin theorem applies. It follows that quantized vortices must originate either on the walls of the container (or on free surface, if one exists), or may exist as closed loops inside the bulk liquid.

D. Superfluid He II under rotation

According to classical fluid mechanics, a container of viscous fluid that rotates at constant angular velocity Ω about the vertical axis has a height profile (neglecting capillary phenomena) given by $z = (\Omega r)^2/(2g)$, where r denotes the radial distance from the axis and g is the acceleration due to gravity; the fluid velocity profile $\boldsymbol{v} = \boldsymbol{\Omega}\hat{\phi}$ matches that of solid body rotation and the

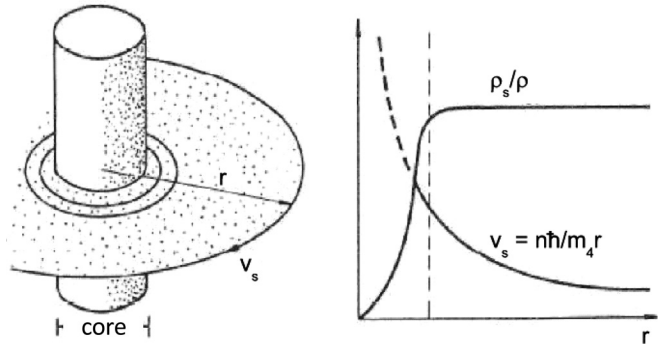

FIG. 4. Left: structure of quantized vortex in He II. Right: superfluid velocity and density profiles in the vicinity of the vortex axis. The vertical dashed line is a measure of the radius of the quantized vortex line. It is of the order of an Angstrom (depending weakly on the pressure and the temperature, except very close to T_λ).

vorticity $\boldsymbol{\omega} = \text{curl}\ \boldsymbol{v} = 2\boldsymbol{\Omega}\hat{z}$, where $\hat{\phi}$ and $\hat{z}$ are the unit vectors along the azimuthal and axial directions, respectively.

For He II, according to the two-fluid model, the restriction curl $\boldsymbol{v}_s$ applies for the superfluid, so at finite temperature one would expect a modified height profile, $z = (\rho_n/\rho)(\Omega r)^2/(2g)$. However, in experiments,[20] the observed profile was classical. It appears that the superfluid component is able to mimic the solid body rotation, due to a hexagonal lattice of rectilinear singly quantized vortices of areal density $n_v = \omega/\kappa = 2\Omega/\kappa$. For characteristic length scales much greater than the distance between quantized vortices we obtain, on average, $\langle \omega_s \rangle = \langle \text{curl}\ \boldsymbol{v}_s \rangle = 2\Omega$.

Although there was hardly any doubt that a lattice of quantized vortices indeed exists in rotating He II (see, e.g., Ref. 21 where photographic technique was used to mark the points where quantized vortices intersect the free surface), its 3D visualization (see Figure 5) *in situ* had eluded for a long time. It is only recently that common classical visualization methods such as particle image velocimetry (PIV) or particle tracking (PT) have been successfully incorporated in He II research. Both fundamental and practical problems have to be solved to use them in He II, especially in finding suitable neutrally buoyant small particles. So far the best option is the use of frozen hydrogen flakes of a few hundred nanometers diameter.[22]

This seminal example of rotating container is conceptually important in understanding the basic principles of QT: just as the lattice of rectilinear vortices is able to mimic solid body rotation, bundles of quantized vortices with the same orientation could mimic turbulent eddies known to exist in classical fluid turbulence.

It is easy to assess (see, e.g., Ref. 15) the condition for the first vortex to appear in the cylindrical vessel of radius R, by minimizing the expression $F' = F - \boldsymbol{L}_a \cdot \boldsymbol{\Omega}$, where F is the free energy and $\boldsymbol{L}_a$ denotes angular momentum of rotating He II. This so-called lower critical velocity is

$$\boldsymbol{\Omega}_c^1 = \frac{\kappa}{R^2} \ln\left(\frac{R}{a_0}\right), \tag{4}$$

and corresponds to what is known as Feynman criterion[2] derived on the basis of similar energy considerations for vortex rings.

It does not mean, however, that upon exceeding this critical velocity quantized vortices necessarily appear in the flow. Nucleation of quantized vortices is a complex problem whose thorough discussion falls outside our present scope. In short, quantized vortices can be nucleated intrinsically (i.e., in a completely vortex-free sample) or extrinsically (i.e., from already existing vortex

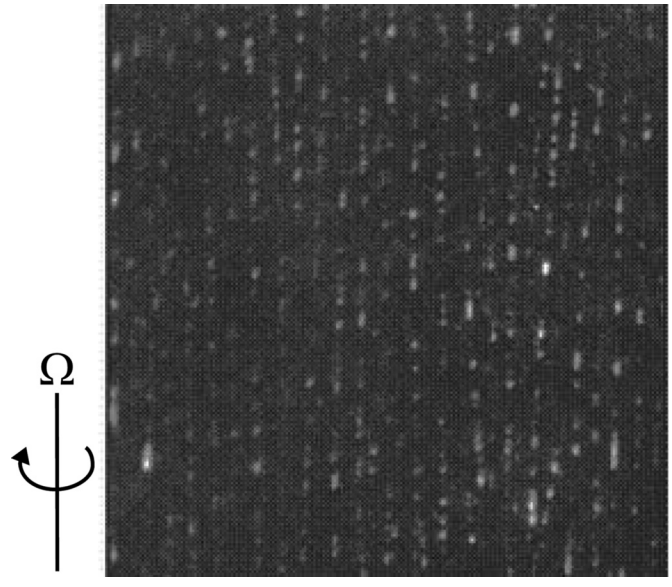

FIG. 5. Photograph of vortex lattice in rotating He II illuminated by laser sheet. The vortices are marked by hydrogen flakes remain trapped by the Magnus force on to cores of quantized vortices.

loops which act as seeds). In any macroscopic sized He II sample, the seeds are always present in practice. Quantized vortices appear spontaneously while cooling the sample through the critical temperature, but decay and disappear at lower temperatures. However, any wall of the container can be considered as rough in comparison with the vortex core size, providing suitable pinning centers for remnant vortices. In fact, it is hardly possible to create any macroscopic He II sample that would be entirely free of remnant vortices. This is why the critical velocities for vortex generation in He II are observed to be low in practice,[23,24] of order few cm/s, rather than of the order of 10 m/s, as it would be required for intrinsic vortex nucleation.

E. Mutual friction

In our discussion on quantized vortices we ignored the normal fluid so far. In fact, quantized vortices interact with phonons and rotons that make up the normal fluid; these quasiparticles are scattered off the vortex cores, giving rise to a mutual friction force. As a result, the normal and superfluid velocity fields are no longer independent, but coupled together. This occurs through the so-called mutual friction, which can be regarded as the friction force on quantized vortices as they move in the normal fluid.

Within the frame of the phenomenological two-fluid model, taking into account the presence of vortices via additional mutual friction coupling terms, and assuming incompressible flow of both components, the equations of motion for the normal fluid and the superfluid are of the form,

$$\begin{aligned}
\rho_s \frac{\partial \boldsymbol{v}_s}{\partial t} + \rho_s(\boldsymbol{v}_s\nabla)\cdot\boldsymbol{v}_s &= -\frac{\rho_s}{\rho}\nabla p + \rho_s S\nabla T + \frac{\rho_n\rho_s}{2\rho}\nabla(\boldsymbol{v}_n-\boldsymbol{v}_s)^2 - \boldsymbol{F}_{ns};\\
\rho_n \frac{\partial \boldsymbol{v}_n}{\partial t} + \rho_n(\boldsymbol{v}_n\nabla)\cdot\boldsymbol{v}_n &= -\frac{\rho_n}{\rho}\nabla p - \rho_s S\nabla T - \frac{\rho_n\rho_s}{2\rho}\nabla(\boldsymbol{v}_n-\boldsymbol{v}_s)^2 + \boldsymbol{F}_{ns} + \eta\nabla^2\boldsymbol{v}_n;
\end{aligned} \tag{5}$$

where η is the dynamic viscosity of the normal fluid, S denotes the entropy of the normal fluid (carrying the entire entropy content of He II) and quadratic terms could in most cases be neglected (except for velocities approaching the second sound velocity, discussed later). The physical meaning of the terms is as follows. The term $\boldsymbol{F}_{\rm ns}$ is the mutual friction term[25] that couples the normal and superfluid velocity fields when quantized vortices are present, even in the case of isothermal flow when the counterflow term $\rho_s S\nabla T$ vanishes. This latter term is responsible for so-called fountain effect. Indeed, with no quantized vortices in a steady flow (i.e., left-hand-side of the two-fluid equations equal to zero) we arrive at the well-known London equation for fountain effect (which was first derived by F. London on the basis of different considerations),

$$\frac{\Delta p}{\Delta T} = \rho S. \tag{6}$$

This equation means that in He II any gradient of temperature leads to a gradient of pressure (and vice versa), as has been verified in many experiments (see, e.g., Ref. 15).

In the simplest case of isothermal flow without vortices, the two-fluid equations reduce to two independent equations of the form,

$$\rho_s \frac{\partial \boldsymbol{v}_s}{\partial t} + \rho_s(\boldsymbol{v}_s\nabla)\cdot\boldsymbol{v}_s = -\frac{\rho_s}{\rho}\nabla p; \tag{7}$$

$$\rho_n \frac{\partial \boldsymbol{v}_n}{\partial t} + \rho_n(\boldsymbol{v}_n\nabla)\cdot\boldsymbol{v}_n = -\frac{\rho_n}{\rho}\nabla p + \eta\nabla^2\boldsymbol{v}_n. \tag{8}$$

The first is Euler equation for the inviscid superfluid (for flow satisfying curl $\boldsymbol{v}_{\rm s}=0$) everywhere, and the second is the Navier-Stokes equation for the normal fluid.

Let us revisit mutual friction, which plays an important role in understanding many features of QT. Mutual friction is best described via its action on second sound, which is the sound mode that exists in He II as a consequence of its two-fluid behavior. The usual longitudinal sound mode in fluids, representing a propagating density wave, also exists in He II, and is termed as first sound. The normal fluid and superfluid oscillate in phase in the first mode and the ratio of the oscillations

remains constant (as does the temperature, defined as their ratio). In the second sound mode, however, the normal fluid and the superfluid oscillate antiphase with each other so that the total density (and pressure) remains constant. Because the entire entropy content is carried by the normal fluid, the second sound is an entropy (or temperature) wave. Indeed, second sound can easily be generated in He II by applying an ac voltage to a resistive heater and detected by a sensitive thermometer.

The motion of normal fluid in the second sound mode is affected (i.e., the second sound wave is attenuated) by quantized vortices: the quasiparticles, namely the phonons and rotons making up the normal fluid, are scattered off the cores of quantized vortices. Hall and Vinen[26] used the rotating second sound resonators with known configuration of the vortex lattice and found that propagation velocity in the presence of vortices stays unaltered to a first approximation, and the second sound is not attenuated if it propagates along the vortex cores. Quantitatively,

$$\boldsymbol{F}_{sn} = B\frac{\rho_s\rho_n}{\rho}\hat{\boldsymbol{\Omega}}\times[\boldsymbol{\Omega}\times(\overline{\boldsymbol{v}}_s-\overline{\boldsymbol{v}}_n)] + B'\frac{\rho_s\rho_n}{\rho}\boldsymbol{\Omega}\times(\overline{\boldsymbol{v}}_s-\overline{\boldsymbol{v}}_n), \tag{9}$$

where $\overline{\boldsymbol{v}}_s$ and $\overline{\boldsymbol{v}}_n$ stand for velocities of flow averaged over a space containing many quantized vortices. The experimentally observed quantities B and B' are weakly dependent on the frequency but are well known and tabulated.[10]

F. Vortex dynamics

Although the existence of quantized vortices is a consequence of quantum mechanics and its clear manifestation on macroscopic scales, resulting also in their quantized circulation, their properties and dynamics can be described classically, except close to their cores. As the cores are of atomic dimension, much smaller than any scale of interest when studying the flow, it is reasonable to approximate them as space curves of infinitesimal thickness, as was done by Schwarz.[27,28] Let $\boldsymbol{s}=\boldsymbol{s}(\xi)$ be the position of a point on such a line, where ξ is the arc length. Denoting as $\boldsymbol{v}_L$ the velocity of vortex line, the forces acting on its unit length are the Magnus force,

$$\boldsymbol{f}_M = \rho_s\boldsymbol{\kappa}\times(\boldsymbol{v}_{\mathrm{L}}-\boldsymbol{v}_s), \tag{10}$$

and the drag force

$$\boldsymbol{f}_D = \rho_s\kappa\alpha\boldsymbol{s}'\times[\boldsymbol{s}'\times(\boldsymbol{v}_s-\boldsymbol{v}_n)] + \alpha'\boldsymbol{s}'\times(\boldsymbol{v}_s-\boldsymbol{v}_n), \tag{11}$$

where $\boldsymbol{\kappa}=\kappa\boldsymbol{s}'=\kappa\hat{\boldsymbol{\omega}}$; $\boldsymbol{s}'=d\boldsymbol{s}/d\xi$ and coefficients α and α' are related to the mutual friction parameters

$$\alpha=\frac{B\rho_n}{2\rho};\quad \alpha'=\frac{B'\rho_n}{2\rho} \tag{12}$$

introduced already. We see that at very low temperature, where the drag force vanishes, the vortex will follow the superflow $\boldsymbol{v}_s$.

We now utilize the analogy of superfluid hydrodynamics and classical electrodynamics mentioned earlier. It follows that the superfluid velocity field is given by the Biot-Savart law,

$$\boldsymbol{v}_s(\boldsymbol{r}_0) = \frac{\kappa}{4\pi}\int\frac{(\boldsymbol{r}-\boldsymbol{r}_0)\times d\boldsymbol{r}}{|\boldsymbol{r}-\boldsymbol{r}_0|^3}, \tag{13}$$

where the integration takes place along all vortex lines. The Biot-Savart law is often difficult for analytical purposes and usually expensive computationally. It is therefore useful to split this integral into the non-local and local contributions. The latter can be expressed as

$$\boldsymbol{v}_s^{\mathrm{loc}}(\boldsymbol{r}) = \frac{\kappa}{4\pi R}\ln\left(\frac{R}{a_{\mathrm{eff}}}\right)\boldsymbol{s}'\times\boldsymbol{s}'', \tag{14}$$

where a_{eff} is the effective core radius and $R=1/|s''|$ is the local radius of curvature. This local contribution is often dominant (especially for the case of counterflow turbulence, see later) and this

Local Induction Approximation that neglects the non-local contribution leads to important and influential results. Let us point out, however, that the non-local contribution is essential for QT generated by methods which are analogous to those of classical turbulence in viscous fluids.

An important example is the deformation of the vortex line. One can show that a deformation of characteristic wavenumber k will propagate along the vortex in a form of a circularly polarized Kelvin wave with the dispersion relation,

$$\mathbf{\Omega} = \frac{\kappa k^2}{4\pi} \ln \frac{1}{k a_0}, \tag{15}$$

where Ω denotes the angular frequency. Note the analogy with vortex waves in conventional fluids—except for the quantized circulation in units of κ this dispersion relation is the same as that derived by Thomson (Lord Kelvin) in 1880.[29] Kelvin waves play an important role in QT. In particular, they may arise in vortex reconnections whose crucial role will be described subsequently.

G. Superfluid phases of ^{3}He

We have already mentioned that differences in quantum statistics lead to great differences between the properties of low temperature ^{3}He and those of ^{4}He. Although ^{3}He also undergoes transition to superfluid state at about $T_c \simeq 1$ mK, the underlying physics is different, rather similar to superconducting transition in metals (superconductivity can be viewed as superfluidity of charged electrons in a crystal lattice) occurring due to so-called Cooper pairing of ^{3}He atoms. Several states of superfluid ^{3}He have been theoretically predicted and experimentally observed. Generally, the superfluid properties of ^{3}He are much more complex than those of He II and their full description falls outside the present scope.

In short, the lower phase diagram in Figure 1 shows the two most common superfluid phases A and B. Various types of quantized vortex structures exist in the strongly anisotropic phase A, including the so-called continuous vortices possessing no hard cores where superfluidity would be suppressed—essentially vortex sheets. Hydrodynamic properties of the A-phase are very interesting and differ in many important ways from He II. We shall, however, not consider them here.

QT has so far been experimentally studied almost exclusively in the B-phase, which in many ways has similar properties to He II. There are, however, important differences. Contrary to liquid He I above the T_λ temperature of extremely low kinematic viscosity, the normal liquid ^{3}He just above its superfluid transition represents a rather thick liquid with viscosity that is comparable to those of air or light industrial oil. This is a consequence of fermionic nature of ^{3}He atoms. Physical properties of normal liquid ^{3}He are described in the frame of so-called Fermi liquid theory developed by Landau[16]; one of its particular features is a steep increase of viscosity $\propto 1/T^2$. As a consequence, within the framework of the two-fluid model, the viscosity of the normal fluid is high, which leads, in most experiments, to the normal fluid that can be considered at rest in the container. The second sound thus does not propagate in ^{3}He, being overdamped by the thick normal component.

Another principal difference arises from the fact that the elementary superfluid particle is not a ^{3}He atom, but the Cooper pair of two ^{3}He atoms rotating about their center of mass. As a consequence, the elementary quantum of circulation is

$$\kappa = \frac{h}{2m_3}, \tag{16}$$

where m_3 denotes the mass of the ^{3}He atom.

Commonly created vortices in ^{3}He B-phase (very different, so-called mass-spin vortices are also possible in some circumstances) are similar to He II vortices described above in that they are singular (that is, they possess hard cores which differ from the bulk B-phase) and singly quantized. The core size, however, is about two orders of magnitude larger than that in He II, of the order of the coherence length in ^{3}He B which, depending on the pressure, ranges from 10 to about 70 μm. Thus the core is a macroscopic object where phase transitions can occur, as was indeed

experimentally observed. Pinning is therefore not always observed, especially in experimental cells made of smooth (e.g., quartz) material. This allows both extrinsic and intrinsic vortex nucleation to occur.

Due to a different dispersion relation (namely, the existence of the energy gap in the energy spectrum), the density of quasiparticles (both quasiparticles and quasiholes are present in this fermionic superfluid) falls with lowering temperature much more steeply—in fact, exponentially—than in He II, and one deals with more or less pure superfluid at temperatures lower than about $0.2\,T_c$.

H. Summary of the phenomenological properties of He II and superfluid ^{3}He

Let us summarize the main flow properties of He II and superfluid ^{3}He-B—our quantum working fluids—from the phenomenological point of view of fluid dynamics.

The two fluids can be prepared at an extremely high level of purity. This is especially true for ^{3}He-B, where at low temperature the efficient self-cleaning process removes all remaining impurities that adhere to walls and the entire bulk sample does not, with huge probability, contain any single impurity including ^{4}He atoms and represents the cleanest substance we have access to. Physical properties of these quantum fluids, which are well known and tabulated, can be changed over several decades *in situ* simply by controlling their temperature and pressure. The intellectually simplest case (though experimentally the most difficult one to attain) is the zero-temperature limit (which, in practice, is below about 0.3 K for He II and below about $0.2\,T_c$ for ^{3}He-B, where T_c varies between about 1 to 2 mK, depending on the pressure), in which both fluids can be treated as pure superfluids. QT occurs here in its simplest form. Based on the above discussion, one might expect in this limit more or less identical properties of QT in He II and ^{3}He-B. From practical point of view, however, given the geometry and experimental restrictions (one of them is a typical energy dissipation rate that is experimentally limited by about 1 W for He II experiments and by about 1 nW for ^{3}He-B experiments) the normal fluid in ^{3}He-B hardly moves and, if it does, the flow remains laminar, while in He II both fluids can become highly turbulent.

III. STEADY-STATE THERMAL COUNTERFLOW TURBULENCE IN He II

Thermal counterflow can be easily set up by applying a voltage to a resistor (heater) located at the closed end of a channel open to a helium bath at the other end, as illustrated in Figure 6. The heat flux $\dot{Q}$ is carried away from the heater by the normal fluid alone, and, by conservation of mass, a superfluid current arises in the opposite direction. In this way a relative (counterflow) velocity $\boldsymbol{v}_{ns} = \boldsymbol{v}_n - \boldsymbol{v}_s$ is created along the channel which is proportional to the applied heat flux, $\dot{q} = \dot{Q}/A$, where A is the cross-section of the flow channel, which for simplicity we assume to be a constant. Assuming that the power $\dot{Q}$ applied at the heater is used to convert superfluid into normal fluid, the velocity of the outgoing normal fluid is

$$v_n = \frac{\dot{q}}{ST\rho}, \tag{17}$$

where S is the specific entropy of He II. The counterflow velocity v_{ns} is then easily evaluated from the condition $\rho_s \boldsymbol{v}_s + \rho_n \boldsymbol{v}_n = 0$. At relatively small values of v_{ns}, the heat transport is affected by

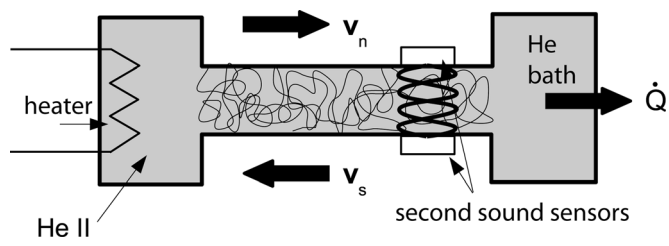

FIG. 6. Schematic view of the generation of counterflow turbulence of He II and its detection using the second sound attenuation method.

turbulence due to the appearance of an apparently disordered tangle of superfluid vortex lines. Its intensity is represented by the vortex line density L, the total length of vortex lines in a unit volume.

Thermal counterflow is peculiar to two-fluid superfluid hydrodynamics (Refs. 15 and 16) and its steady state has no obvious analog in flows of ordinary viscous fluid. For this reason it was often stated that counterflow turbulence in He II has nothing to do with classical turbulence in viscous fluids, but recent experiments suggest otherwise. Clearly, if one attempted to find a possible connection between thermal counterflow and classical turbulence, the likely candidate would be turbulent thermal convection, but this link is yet to be investigated thoroughly. In fact, as noticed by Skrbek, Gordeev, and Soukup,[30] the turbulent heat transport in both cases is strikingly similar, having a power law dependence on the temperature difference with an exponent that is close to 1/3.

A. Historical remarks

Experimentally, counterflow turbulence in He II has a long history since the discovery of superfluidity, beginning with the heat transport experiments through capillaries and channels of various sizes. It was observed by Gorter and Mellink[31] that, in wide channels with flow velocities that are not very low, there is a dissipative process due to the mutual friction force between the normal fluid and superfluid, of the form $A\rho_s\rho_n(v_s - v_n)^3$ per unit volume. The origin of this process was not known at that time, but it became clear in the fifties (thanks to the ideas of Onsager[18] and Feynman[2]) that the mutual friction is the result of interaction between the normal fluid and quantized vortices.

We shall describe only a few experimental results here and, for an excellent review of early results, direct the reader to Tough[23]; scaling and dynamical similarity in turbulent counterflowing He II based on experimental results available up to 1985 is discussed in detail by Swanson and Donnelly.[32] Counterflow turbulence in a wide channel was first investigated in detail in an outstanding series of papers by Vinen,[5] who also introduced for its description a phenomenological model based on the concept of a random vortex tangle characterized by the approximately homogeneous vortex line density L. He argued that L (which has the dimensions of length per volume) obeys the following equation (now called Vinen's equation),

$$\frac{dL}{dt} = \frac{\rho_n B}{2\rho}\chi_1 v_{ns} L^{3/2} + g(v_{ns}) - \frac{\kappa}{2\pi}\chi_2 L^2, \tag{18}$$

where ρ and ρ_n are the total and normal fluid densities, κ is the circulation quantum, χ_1, χ_2 are undetermined dimensionless constants and B is the mutual friction parameter, tabulated in Ref. 10. The arguments leading to Eq. (18) are dimensional: The first term on the right hand side describes the production of turbulence, the last term its decay. The unspecified function $g(v_{ns})$ (note that for dimensional reasons g must depend also on κ) had to be included to comply with the experimental fact that there are no quantized vortices, hence no mutual friction, below certain critical value of v_{ns}.

Equation (18) was later deduced, under a number of assumptions, by Schwarz[28] using the laws of vortex dynamics in the local induction approximation introduced earlier. Under the assumption that the vortex tangle is homogeneous and the quantity L is adequate to characterize it—from the point of view of turbulence, this means that there is only one relevant length scale, $\ell_v = 1/\sqrt{L}$, namely the average distance between the quantized vortices—this approach accounts for most of the observed phenomena in steady state counterflow turbulence, as described by Tough,[23] whose group contributed a great deal to the experimental investigation of counterflow in He II. Assuming that $g(v_{ns})$ is small, the steady-state solution of Vinen's equation yields

$$L^{1/2} = \frac{\pi\rho_n B\chi_1}{\rho\kappa\chi_2} v_{ns}, \tag{19}$$

which means that L is proportional to the square of the counterflow velocity; its steady-state value determines only the ratio χ_1/χ_2.

The relative increase over the counterflow channel length of temperature ΔT, pressure Δp, and the chemical potential $\Delta\mu$, as well as the influence of the counterflow on the transmission of positive and negative ions, have been measured by various investigators, using powerful techniques besides second sound attenuation. For details of these techniques, we direct the reader to the review by Tough[23] and original references therein.

B. Some experimental details of steady-state thermal counterflow turbulence in He II

When a heater situated at the end of the counterflow channel, such as shown in Figure 6, is switched on, it does not take long before a steady-state counterflow gets established. When the applied power density $\dot{q} = \dot{Q}/A$ is below a critical value, there are no quantized vortices in the flow (except for the remnant ones). The normal fluid and superfluid velocity fields are not affected by the mutual friction force; therefore the normal fluid behaves as an ordinary viscous fluid of viscosity η, and its flow acquires the usual parabolic profile with a Δp that agrees with the Poiseuille formula for laminar flow,

$$\Delta p_{\text{lam}} = G\eta\ell v_n/d^2, \tag{20}$$

where G is a factor generally known for a particular channel geometry, ℓ is its length, and d denotes the channel height (the smaller dimension). The temperature difference ΔT is naturally determined by Δp via the London equation (6) discussed in the previous section, and yields

$$\Delta T_{\text{lam}} = \Delta p/\rho S = G\eta\ell v_n/\rho S d^2. \tag{21}$$

The steady counterflow turbulence becomes established when the applied power $\dot{q}$ exceeds the critical value. The pressure difference Δp_{turb} as a function of $\dot{q}$ only slightly exceeds the extrapolation of the laminar data—this being the so-called Allen-Reekie rule.[33] On the other hand, the chemical potential and temperature difference increase dramatically in the turbulent state, and are found to exceed their laminar values in rough proportion to $\dot{q}^3$. The increased dissipation in the turbulent state can be described by a dissipative mutual friction force which also gives rise to an excess second sound attenuation, increasing approximately as $\dot{q}^2$.[5]

We have already mentioned that the microscopic origin of the mutual friction force is the scattering of the elementary excitations, the phonons, and the rotons (i.e., the normal fluid), off the quantized vortex lines. The important question is the form of distribution of these vortex lines. To obtain at least a partial answer to this question, ion currents have been explored. Positive helium ions are effectively solid snowballs made of about 20 helium atoms while negative helium ions represent effectively an electron in otherwise empty bubble of a nanometer size, possessing a rather large hydrodynamic added mass of order 200 bare helium atoms. The motion of both ion species can be controlled by an externally applied electric field and is affected by the presence of quantized vortices. Due to the superfluid pressure gradient owing to superfluid circulation, an attractive interaction exists between the ions and the vortices, capable of trapping the ions on the vortex cores.

Negative ions have been successfully used by Awschalom, Milliken, and Schwarz[34] to probe the local properties of counterflow turbulence in a large channel of $1\,\text{cm} \times 2.3\,\text{cm}$ rectangular crossection, as shown in Figure 7. They used pulsed-ion technique based on the tritium source to obtain the spatially resolved measurements of the vortex line density and the normal fluid velocity field in turbulent counterflow. In their measurements, a narrow pulse of negative ions was gated into the channel and allowed to propagate to a particular position under the action of an applied electric field. The field was then switched off, allowing the pulse to remain at this position for as long as several seconds. Some of the ions in the pulse were trapped by quantized vortices; the rest drifted along with the local normal fluid velocity. Later, the electric field was turned back on and the surviving pulse was measured in real time by means of one or more electrometers, as it arrived at one of three collectors on the opposite side of the channel, positioned along the channel axis. From the amplitude of the observed pulse and where it fell on the collector, the local values of L and v_n were determined, with a spatial accuracy better than 1 mm, providing what is up to now probably the best information on the local structure of counterflow He II turbulence. The

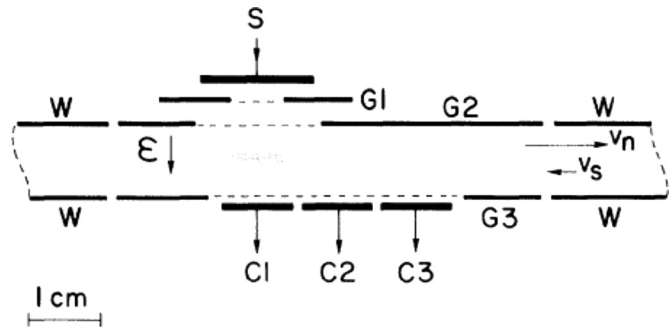

FIG. 7. Experimental arrangement of Awschalom, Milliken and Schwarz.[34] S denotes the tritium ion source, G1, G2, G3 are pulsed grids, C1, C2, C3 are collectors, W denotes the channel wall, v_s and v_n in the counterflow are indicated by arrows. The dotted region indicates a typical ion pulse; the ions are moved by an electric field ε.

remarkable result was that within the experimental uncertainty of up to few percent L was found constant over entire crosssection of the channel, except within about 1 mm from the walls where the technique fails. The conclusion was that in counterflow turbulence the normal fluid profile is approximately flat (except close to the walls, see later) and the vortex line density is approximately homogeneous.

C. TI, TII, and TIII states of counterflow turbulence in He II

Careful and extensive measurements of the temperature difference along the counterflow channel of Tough's group[23] clearly indicate that, depending on the geometry, there are several steady counterflow turbulent states. In rather large channels of circular or square crosssection, upon increasing the applied power per unit area of the channel, $\dot{q}$, the laminar flow undergoes the first transition at $\dot{q}_{c1}$, above which the measured ΔT exceeds the extrapolated laminar value only slightly, until at $\dot{q}_{c2}$ the second transition occurs, above which the measured ΔT is dramatically enhanced. These turbulent states are referred to as TI and TII.

The existence of the state TI for $\dot{q}_{c1} < \dot{q}_{c1} < \dot{q}_{c2}$ was recognized by early workers thanks to its signature in the second sound attenuation data of Vinen,[5] the pressure difference data of Brewer and Edwards,[35] and the temperature difference data by Chase.[36] But it was experimentally investigated in greater detail by Tough's group. Much less is known about TI than about the state TII (especially about the scaling of observed variables with the applied heat flux), as it exists only in the rather narrow, temperature-dependent, region $\dot{q}_{c1} < \dot{q}_{c1} < \dot{q}_{c2}$. Because the agreement between the experimental data and the homogeneous theory is worse in TI than in TII (for which this theory works rather well), it was claimed in Ref. 23 that the TI state might not be homogeneous and isotropic. Recently, however, Adachi, Fujiyama, and Tsubota[37] performed vortex filament simulations on steady-state counterflow turbulence using the full Biot-Savart law and compared the results with the simulations of Schwarz[28] and their own, based on local induction approximation. They claim that local induction approximation is not suitable for simulations of turbulence, as such calculations constructs a layered structure of vortices and does not proceed to a turbulent state, a problem which was somewhat artificially solved by Schwarz in his original calculations. While it is clear that the full Biot-Savart approach is certainly better, there are still other aspects such as approach to vortex reconnections and influence of possible normal fluid turbulence that make the predictive power of these simulations limited at the best.

There is a profound effect of geometry on counterflow turbulence. In channels of high aspect ratio (1:10) rectangular cross section with a small dimension below 100 μm only one transition has been observed at $\dot{q}_{c3}$. This steady-state turbulence is denoted by Tough as TIII.

No hysteresis associated with the TI-TII transition has been observed, but metastable laminar states can be observed for heat fluxes considerably larger than $\dot{q}_{c1}$ or $\dot{q}_{c3}$. However, large fluctuations of the chemical potential and temperature difference have been observed in the vicinity of the TI-TII transition.

The existence of the two distinctly different steady turbulent states in He II counterflow turbulence has been a long-standing puzzle. One possibility to understand this problem was

considered by Melotte and Barenghi,[38] who addressed the issue of the velocity profile of the normal fluid and its stability. The calculation suggests that the superfluid is turbulent in the TI state but the normal fluid is still laminar. The TI to TII transition might thus correspond to the onset of the normal fluid turbulence.

D. Visualization of thermal counterflow turbulence in He II

Very interesting results have recently been obtained by particle image velocimetry and particle tracking visualization techniques[39,40] in steady counterflow of He II. The interpretation of these experiments is complex because of the two-fluid behavior of He II, which makes it difficult to state with confidence which velocity field is being tracked by the particles. We direct the reader to the recent review by Sergeev and Barenghi,[41] with a number of original references. Van Sciver, Fuzier, and Xu[39] used the PIV technique based on solid polymer spheres 1.7 μm in size. As shown in Figure 8, the observed particles velocities are roughly equal to half of the expected normal fluid velocity, at all temperatures. This puzzling result could be understood by the fact that relatively big particles are not fully trapped by quantized vortices but slowed down when they are being carried (due to Stokes force) by the viscous normal fluid.

Qualitatively new results have been achieved by Paoletti *et al.*[40] They used smaller particles—flakes of solid hydrogen—and used particle tracking methods. The observed trajectories in vertical counterflow are shown in Figure 9. Because the characters of these trajectories are clearly qualitatively different, there appears to be no doubt that two different velocity fields have been mapped for the first time.

It is useful to study the probability density functions of the observed particle velocities (see Figure 10). For classical homogeneous turbulence in a viscous fluid such as water one expects PDFs of nearly Gaussian form. We see, however, that both horizontal and vertical velocity distributions are much less steep and roughly follow power law of exponent about −3. Note in passing that very recently similar power law nonclassical velocity statistics have been found theoretically by White *et al.*[42] in 2D trapped and 3D homogeneous Bose-Einstein condensates and in classical 2D vortex points systems. One has to interpret these results with care,[40] but it is clear that in counterflow turbulence the statistical weight of large velocity fluctuations significantly exceeds that in classical homogeneous turbulence.

Very recently a new visualization technique has been developed and successfully applied to study counterflow in He II by Guo *et al.*[43] The technique consists in imaging the motion of tagged

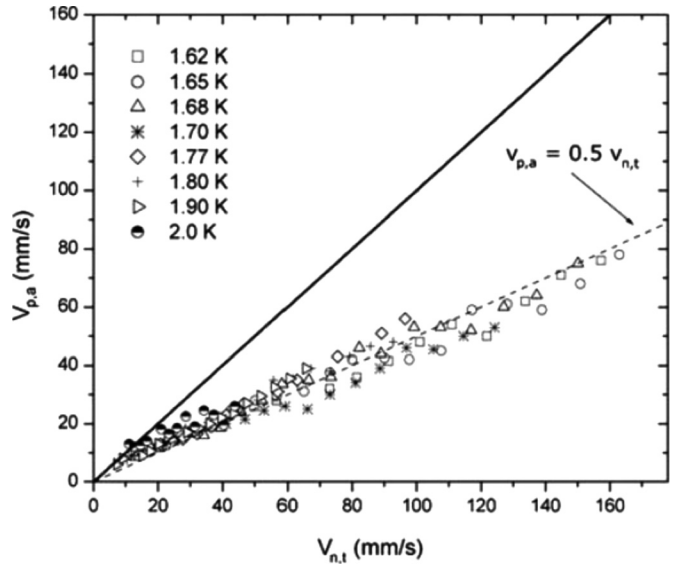

FIG. 8. The observed velocities of tracking particles plotted versus calculated normal fluid velocity at temperatures as indicated.[39]

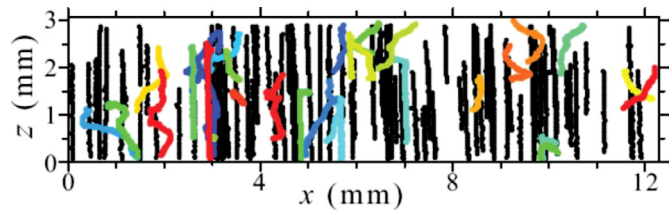

FIG. 9. (Color online) The observed trajectories of tracking particles in counterflowing He II.[40] The regular (straight, black) trajectories are those of particles moving with the normal fluid, while irregular trajectories (colored) in the opposite direction are those of particles trapped in vortex cores.

metastable helium molecules $-He_2^*$ triplet molecules with a radiative lifetime of about 13 s—using a laser-induced fluorescence.[44] Because of their small size, at $T > 1$ K (the experiments were so far performed at 1.8 K and 1.95 K), they are not trapped into the cores of quantized vortices and act as tracers that follow the motion of the normal fluid. For high heat fluxes, Eq. (17) for the normal fluid velocity was directly confirmed experimentally for the first time. This supports the point of view that the normal fluid is turbulent under such conditions and its flow profile is flat. For low heat fluxes, however, when both superfluid and normal fluid are in a laminar flow state, the normal fluid velocity in the middle of the channel was found to be about twice of that calculated by Eq. (17), which strongly supports a Poiseuille profile. This new technique is potentially very powerful—for example, a line of such molecules can be created inside the observation region and its motion and deformation can be followed for a wide range of applied heat fluxes.

IV. DECAYING COUNTERFLOW TURBULENCE IN He II

Vinen's equation (18) has also been tested in the case of time dependent flows. If the power applied to the heater has a white noise frequency spectrum, the spectral response of L can be derived from Vinen's equation. The result agrees well with the experiment of Barenghi, Swanson, and Donnelly.[45] One can then combine steady-state measurement with those of the spectrum and determine χ_1 and χ_2, separately. Vinen's equation can be applied also to the transient response of the vortex tangle from one steady state to another. It even allows an analytical solution, as shown by Schwarz and Rozen.[46] For free temporal decay, setting $v_{ns} = 0$, the solution of Eq. (18) reduces to the inverse time dependence $L(t) \propto 1/(t + t_{vo})$, where t_{vo} stands for the virtual origin in time. We shall see, however, that this simple prediction does not hold in most cases, as the decaying counterflow turbulence involves additional physical processes closely connected to classical hydrodynamic turbulence.

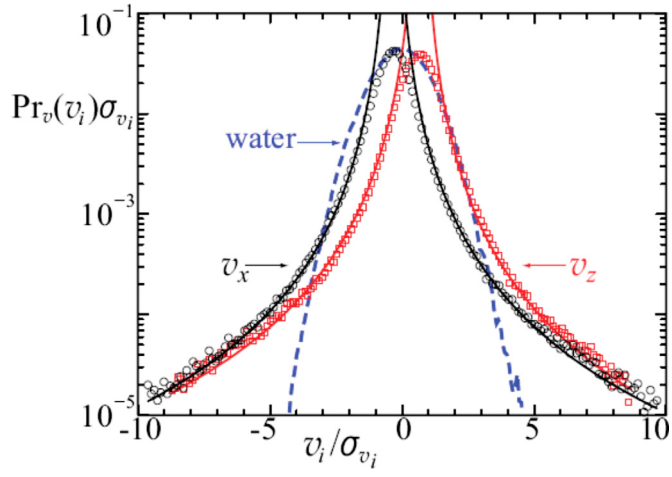

FIG. 10. (Color online) The probability density function of observed horizontal (v_x) and vertical (v_z, red) velocities appears very different from the expected conventional PDF of Gaussian form found in classical viscous fluid.[40]

A. Thermally-driven decay versus isothermal decay

Before analyzing the temporal decay of the vortex tangle generated in counterflow, it is useful to estimate the characteristic time τ for the decay of the temperature difference ΔT across the counterflow channel using simple thermodynamic consideration.[47] Gordeev *et al.*[47] assumed a channel of constant crosssection A and length ℓ and, for simplicity, a linear temperature variation along the channel length, $\nabla T = \Delta T/\ell$. When the heat input $\dot{Q}$ applied to its closed end is switched off, the amount of heat that must be taken away from the end into the bath kept at the temperature T_0 equals $Q_{ch} = c\varrho A\ell^2 \nabla T/2$ (for linear ∇T, the average excess temperature over the entire channel is not ΔT but $\Delta T/2$), where $c(T) \cong c(T_0) = c$ is the specific heat of He II (if there is an additional volume V adjacent to the hot end of the channel in which the heater is placed, we have to add the heat $Q_V = c\varrho V\ell\nabla T$). Thus the total excess heat equals to $Q = Q_{ch} + Q_V = c\varrho\ell(A\ell + 2V)\nabla T/2$. Differentiation with respect of time gives

$$\frac{dQ}{dt} = \dot{Q} = c\varrho\ell(A\ell + 2V)\,(\dot{\nabla T})\,/2. \tag{22}$$

On the other hand, as established already by Vinen,[5] for high enough counterflow velocity,

$$\dot{Q} = -A\zeta(T)(\nabla T)^{1/3}, \tag{23}$$

where ζ is a temperature dependent heat efficiency parameter. Equations (22) and (23) provide a differential equation for $\nabla T(t)$, which is easy to solve by separating the variables,

$$[\nabla T(t)]^{2/3} = [\nabla T(0)]^{2/3} - \frac{4\zeta A}{3c\varrho\ell(A\ell + 2V)}\,t. \tag{24}$$

Here $\nabla T(0)$ is the initial temperature gradient, measured in the steady state before the heater is switched off. Defining τ from Eq. (24) as the time when $\nabla T(t) \to 0$, we have

$$\tau = \frac{3c\varrho\ell(A\ell + 2V)}{4\zeta A}\,[\nabla T(0)]^{2/3}. \tag{25}$$

Figure 11 applies these simple considerations to the original experiment of Vinen.[5] It shows the scan of the original experimental data, on which is superimposed the linear time dependence predicted by Eq. (24). This procedure is reasonable, as the excess attenuation of the second sound in the steady state was experimentally found to be proportional to $\dot{Q}^2$ and hence also to $[\nabla T(t)]^{2/3}$. The quantitative agreement between the data and this simple approach allows dividing the decay into two distinctly different parts:

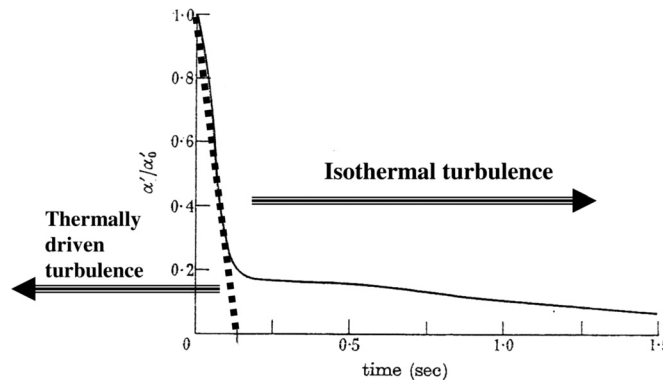

FIG. 11. Variation with time of the excess second sound attenuation α'/α'_0 after a heat current 0.14 W/cm^2 has been switched off.[5] α'_0 is the attenuation in the steady heat current. The dotted line is a plot of Eq. (24), with τ estimated to be about 0.14 s, based on the geometry of the apparatus.

(i) $t < \tau$, where the decaying turbulence is still thermally driven by the excess heat accumulated in the hot end of the flow channel and

(ii) $t > \tau$, where the decaying turbulence can be treated as approximately isothermal.

It follows from formula (25) that τ is long if there is a big buffer volume V adjacent to the hot end of the channel and/or if the counterflow channel is very long. Here, the decay of counterflow can be understood as a sequence of steady states, wherein the dynamics of decaying turbulence is suppressed. These simple thermodynamic considerations are important when analyzing the transient behavior, or the free decay of counterflow turbulence experimentally investigated by various authors. We suggest that the procedure just outlined might be useful for analyzing the decay of turbulent thermal convection in classical viscous fluids.

B. Isothermal decay of counterflow turbulence

The powerful technique of second sound attenuation is capable of direct investigation of rather complex physics of the decaying counterflow turbulence even when it can be considered approximately isothermal. A typical family of decay curves[47] is shown in Figure 12. The most striking feature is that the late stage of the decay of turbulence displays the classical $t^{-3/2}$ power law, independently of temperature (a derivation of this result for classical turbulence is discussed later).

The measurement of decaying counterflow turbulence in two channels of square cross-section[47] provided a first direct experimental check that the vortex line density in the late stage of the decay is proportional to the channel size D. The early part of the isothermal decay, on the other hand, displays complicated features; the decay is slow and sometimes even includes periods during which the second sound signal appears to increase rather than decrease, which (under assumption of isotropic and homogeneous tangle) would imply a puzzling increase of vortex line density. We shall discuss these features together with other data on decaying vortex line density in QT.

V. QT IN CO-FLOWS OF He II ABOVE ABOUT 1 K

In this section we consider situations when the two fluids constituting He II flow, on the average, in the same direction (or there is no mean flow); classical analogues may in principle be

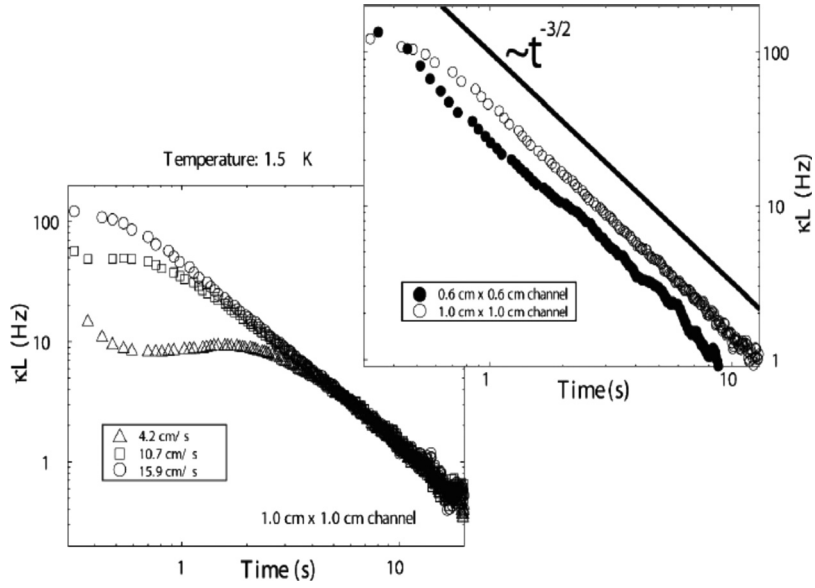

FIG. 12. Log-log plots of decaying vortex line density $L(t)$, deduced from the relaxing amplitude of the second sound under the assumption of random vortex tangle.[47] The early decay period depends on initial counterflow velocity and may even include a period of increasing $L(t)$, but eventually all decay curves closely follow power law decay $\kappa L = \beta t^{-3/2}$, where the temperature-dependent prefactor $\beta(T)$ does not depend on initial conditions but appears to be proportional to the channel size.

possible in this instance (unlike for the counterflow case). This flow regime is referred to as co-flow. We consider temperatures above about 1 K, where both the normal fluid and the superfluid are present, though in varying proportions (becoming entirely normal above $T_\lambda \approx 2.17$ K). Below about 1 K, there is hardly any normal fluid, as rotons and phonons—quasiparticles making up the normal fluid—are frozen out. As we shall see, due to quantum mechanical restrictions, a perfect co-flow regime is not possible at all length scales but is restricted to those that are large in comparison to the average distance between quantized vortices. Given that the general theory is absent, the topic is led mostly by experiments and phenomenology.

A. Counterrotating discs in He II above 1 K

Let us start with important and informative experiment of Maurer and Tabeling,[6] who measured the frequency spectrum of local pressure fluctuations in liquid helium using a total-head pressure tube. Measurements were made in both classical and quantum turbulence generated between counterrotating discs with blades, using He I and He II. Pressure fluctuations were measured at a location with non-zero mean flow, thus measuring mostly fluctuations of the pressure head, which in turn are present due to velocity fluctuations. The measurements thus can be related to the turbulent energy spectrum in the frequency domain; stretching the imagination a bit, the frequency spectrum can be related, via Taylor's frozen flow hypothesis, to the energy spectral density $\phi(k)$. The striking results are that (a) there are no detectable changes in the form of the spectrum over the whole range of the relevant temperature (1.4 K to 2.3 K—liquid helium is largely superfluid at 1.4 K and entirely normal at 2.3 K) and (b) over the range of relevant wavenumbers detected by the total-head tube (limited mainly by its size due to organ pipe resonance), the spectrum is of the Kolmogorov form within measurement accuracy (see Figure 13). Moreover, the numerical value of the Kolmogorov constant was $C \cong 1.5$, well within the range of accepted classical values[48] $C = 1.62 \pm 0.17$. Even the intermittency corrections deduced by further analysis remained independent of the fraction of the normal to superfluid components. A simple explanation of this result is that at scales to which this experiment had access, the two fluids move with the velocity field that is identical with that expected in the classical turbulent case.

The 1998 experiment of Maurer and Tabeling[6] in a turbulent Von Kármán flow, namely observation of the classical Kolmogorov form of the spectral energy density has not been experimentally confirmed for a long time, until very recently. The confirmation follows systematic

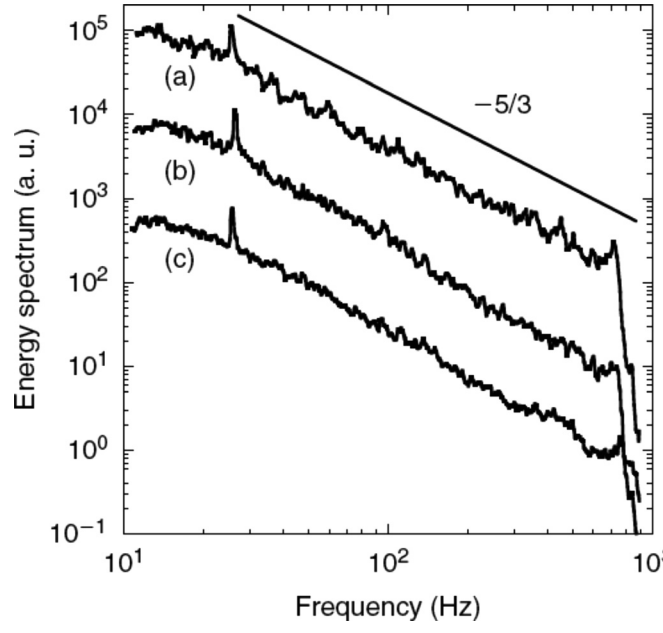

FIG. 13. The measured energy spectral density in a flow of liquid helium confined between counterrotating discs at temperatures 2.3 K (a), 2.08 K (b), and 1.4 K (c).[6] For further details (see the text).

measurements in different highly turbulent flows of cryogenic helium: grid and wake flows in a pressurized wind tunnel capable of achieving mean velocities up to 5 m/s both above and below the superfluid transition down to 1.7 K, and a "chunk" turbulence flow at 1.55 K, capable of sustaining mean superflow velocities up to 1.3 m/s. The upper inertial range of the turbulent cascade was resolved with various anemometers based on stagnation pressure probes. The authors of Ref. 49 claim that the second order statistics of the superfluid velocity fluctuations indeed does not seem to differ from those of classical turbulence down to the precision of their measurements. Further details of this important large scale activity of a number of French researchers[49] will have to await original research publications.

B. Grid turbulence in He II

The properties of steady state and the decay of the nearly homogeneous and isotropic turbulence (HIT) generated behind grids in air and water is one of the basic and extensively explored problems in turbulence. Most of the experimental work has occurred in wind tunnels, where the turbulence is studied as it decays downstream (e.g., Refs. 50–52). Turbulence without a mean flow, generated by using an oscillating grid (e.g., Ref. 53) and by towing a grid through a stationary sample of fluid (e.g., Ref. 54) has also been studied. A general theory describing the decay of turbulence based on first principles has not yet been developed. However, the works of Comte-Bellot and Corrsin[51] and Saffman[55]) outline a phenomenological theory relating the forms of the three-dimensional turbulent energy spectra uniquely to the temporal decay of turbulence. This approach was extended by Skrbek and Stalp,[56] by taking into account ideas of Eyink and Thomson,[57] to include the finite size of the turbulence-generating box, intermittency and viscosity effects. Rather surprisingly, under certain reasonable assumptions, classical decay models describe very well a variety of experimental data on decaying vortex line density in decaying quantum turbulence. We first discuss the relevant experiments and methods for deducing the decaying vortex line density, which for QT is the quantity of primary interest.

C. Oregon towed grid experiments in He II

Experiments on decaying quantum turbulence in He II generated by the towed grid have been performed over many years in Donnelly's group in Oregon. The experimental results have been published in a series of papers.[7,8,58–60] The schematic of the apparatus is shown in Figure 14. The turbulence is generated by towing a grid through a stationary sample of He II contained in a channel of square crosssection (about 29 cm long and $D = 1$ cm wide, manufactured by an electroforming process). Two different grids have been used over time. The first was of unconventional design—a 65% open brass monoplanar grid of rectangular tines, 1.5 mm thick, with a mesh size, M (tine spacing) of 0.167 cm; the second, consisting of 28 rectangular tines of width 0.012 cm forming 13×13 full meshes across the channel of approximate dimension $M = 0.064$ cm, was identical in design to that of Comte-Bellot and Corrsin.[51] The grid was attached to a stainless steel pulling rod which exited the cryostat via a pair of tight sliding seals. The space between the seals was continually evacuated to prevent the introduction of impurities inside the cryostat during the experiment. Above the cryostat, the rod was attached to a computer controlled linear servo motor that positioned the grid with the accuracy of about 1 mm and provided the towing velocity, v_g, up to 2.5 m/s. This arrangement enabled the exploration of a wide range of mesh Reynolds numbers up to $Re_M = v_g M\rho/\mu \leq 2 \times 10^5$, where μ is the dynamic viscosity of the normal fluid and ρ the total density. The channel was suspended vertically in the helium cryostat and totally submersed in superfluid helium during the measurement, and entered the cryostat via 16 holes, 500 μm in diameter, placed near the top end. Except for these tiny holes, the channel was leak-tight.

To probe the vortex line density, L, resulting from pulling the grid through the channel, the second sound attenuation technique was used. Second sound was excited and detected using vibrating nuclepore membranes 9 mm in diameter mounted flush on opposing walls of the channel. These 6 μm thick polycarbonate membranes have a dense distribution of 0.1 μm holes. On one side about 100 Å thick layer of gold was evaporated and pressed against a container wall. This gold layer forms an electrode of a capacitor transducer, with the other being a brass electrode

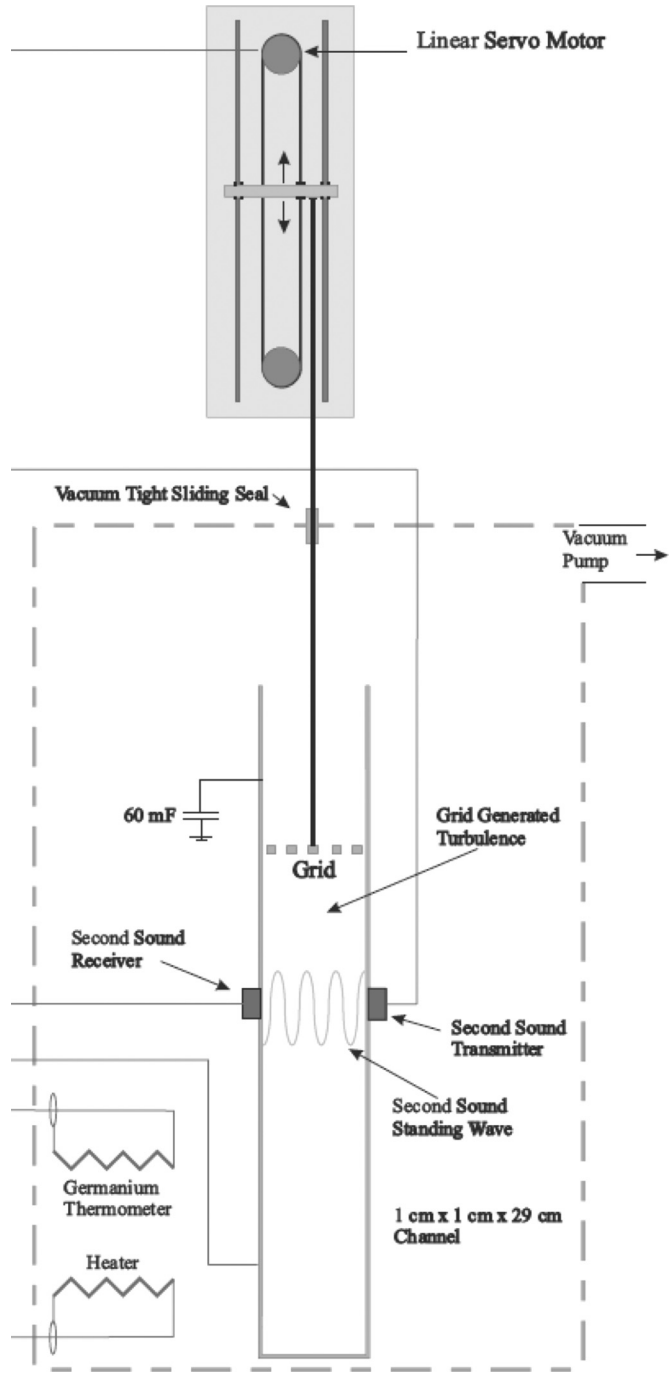

FIG. 14. Schematic of the experimental apparatus.

pressed towards the opposite side of the membrane from outside the channel. By applying an ac signal ($\sim 0.3 - 1\ V_{PP}$) in addition to a dc bias ($\sim 100\ V$), one obtains an oscillatory motion of the membrane. In He II, the normal fluid is clamped by viscosity inside the small holes of the membrane, while the superfluid component passes freely, thereby exciting second sound. Directly across the channel the second sound wave produces a corresponding oscillation of the other membrane (i.e., the receiver) and the induced signal is input to a lock-in amplifier referenced to the transmitter frequency. The channel itself acts as a second sound resonator. The excitation amplitude is adjusted to be within the upper half of the linear response range and the n-th harmonic, with n about 50, of the fundamental frequency, typically 30–40 kHz, is used. A Lorentzian

resonance peak is obtained, whose width at half maximum is temperature dependent and typically reaches values of $\Delta_0 = 20$–500 Hz in the absence of quantized vortices in the channel.

The data acquisition process is as follows. The cryostat was filled with liquid helium, the bath being pumped and temperature controlled as desired. With the grid "parked" towards the top of the channel, the second sound resonance curve was measured and fitted to a Lorentzian, giving the linewidth Δ_0. The grid was then lowered to the bottom and, after a necessary waiting time ($\approx$2 minutes), pulled through the channel with constant velocity and equal v_g for at least 5 cm below and above the experimental volume. It was then slowed down and smoothly "parked" at the top again. The data acquisition was triggered when the grid passed a predetermined position of 2 mm above the measuring volume, as determined by a signal from a photodiode. Typically 100 s of data were recorded at a rate of 100 Hz from the output signal of the lock-in amplifier, representing the recovering wave amplitude of the second sound standing wave. Under the assumption that the vortex tangle is random, the amplitude may be converted to decaying vortex line density. Typical family of decay curves is shown in Figure 15.

To understand the use of second sound in detecting the vortex line density, we return to the seminal work of Hall and Vinen.[26] In experiments with a rotating container of He II, they observed an excess attenuation of second sound in a direction perpendicular to the rotation axis due to the presence of quantized vortices, $\alpha_L = B\Omega/2u_2$, where Ω is the rotation rate of the container, u_2 is the second sound velocity and B is a temperature dependent (and weakly frequency dependent) mutual friction coefficient.[10] In rotating container, the vorticity $\omega = 2\Omega = \kappa L$, where κ is the circulation quantum ($\kappa = h/m_4$, h being Planck's constant and m_4 the mass of the helium atom).

By considering a second sound resonance as an infinite series of reflected waves in a rotating cavity, the extra attenuation (in a limit of small values) due to quantized vortices becomes[8,61]

$$\alpha_L = \frac{B\kappa L}{4u_2} = \frac{\pi\Delta_0}{u_2}\left(\frac{a_0}{a} - 1\right), \tag{26}$$

where a and a_0 are, respectively, the amplitudes of the standing wave resonance of the second sound, with and without vortices present.

What is detected by the second sound sensors, however, is neither the total vortex length, nor the individual projected lengths. It can be shown[62] that the attenuation of a second sound wave of

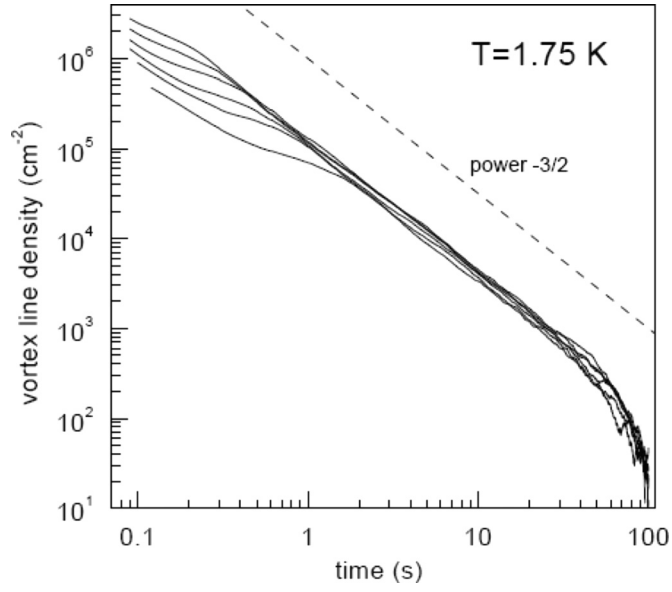

FIG. 15. The log-log plot of the decaying vortex line density versus time after grid passes 2 mm above the measuring volume. Each decay curve represents an average of three identical pulls. The decay curves, in order, correspond to mesh Reynolds number $Re_M = 2 \times 10^5$ (the uppermost one), 1.5×10^5, 10^5, 5×10^4, 2.5×10^4, 10^4, 5×10^3, and 2×10^3. For each Re_M, the decaying vortex density joins and follows thereafter the universal power decay with exponent $-3/2$.[61]

angular frequency ω in the presence of a straight vortex line is $\sin^2(\theta)\omega B/(2\Omega)$ where θ is the angle between the direction of the quantized vorticity and the direction of second sound propagation. This "sine squared law" has been confirmed experimentally by measuring second sound signals in a container of helium held at tilted angles with respect to the axis of rotation of the cryostat.[63,64] If the tangle is assumed isotropic, since $\langle \sin^2(\gamma) \rangle = 2/3$ where $\langle\ \rangle$ denotes the average over the unit sphere, the second sound sensors detect $L_{\rm eff} = 2L/3$, where L is the actual vortex line density.

Equation (26) can be extended to the case of a homogeneous vortex tangle, taking into account the fact that vortices oriented parallel to the second sound propagation do not contribute to the excess attenuation. We then have

$$L = \frac{6\pi\Delta_0}{B\kappa}\left(\frac{a_0}{a} - 1\right). \tag{27}$$

Let $p = a_0/a$ and $P = 1 - \cos(2\pi d\Delta_0/u_2)$. For small $d\Delta_0/u_2$, it can then be shown that a more precise formula is

$$L = \frac{3u_2}{B\kappa d}\ln\left[\frac{1 + p^2P + \sqrt{2p^2P + p^4P^2}}{1 + P + \sqrt{2P + P^2}}\right]. \tag{28}$$

The previous two equations differ from that written by Stalp in Ref. 61, where the sine squared law was not taken into account. All values of L reported in the Oregon towed grid experiments (and some Prague decaying counterflow experiments, see later) must thus be multiplied by a factor of $3\pi/8 \approx 1.2$.

VI. QT IN THE ZERO-TEMPERATURE LIMIT

We recall from the Introduction that both He II and ^{3}He-B can be considered as consisting of the pure superfluid in this limit. In particular, there is neither classical viscosity nor viscous forces. Therefore, for a first approximation, we expect that QT in these two fluids will bear the same features and serve as a simplest prototype of turbulence in fluids, consisting of a tangle of singly quantized vortex line. From the experimental point of view, however, this limit represents a challenge, for several reasons.

First, reaching these temperatures, cooling down big enough samples of these fluids and measuring their temperature require special approaches and techniques such as dilution refrigerators and nuclear demagnetization cryostats. Second, the second sound attenuation method that proved so powerful in He II above about 1 K cannot be used here (second sound simply does not exist if there is no normal fluid) and adequate flow visualization methods (although there seem to be no principle difficulties to apply them) capable of producing reliable *quantitative* data are yet to be developed at these temperatures.

A very useful tool which works in principle at any temperature is to use helium ions. As in counterflow turbulence mentioned above,[34] bare helium ions have been successfully used by Milliken, Schwarz, and Smith[65] to investigate the decay of inhomogeneous QT created by ultrasonic transducers in superfluid ^{4}He at about 1.5 K in early eighties (see later).

Vibrating structures such as discs,[17] spheres, grids, and wires have been widely used in research on quantum fluids since the beginning of this field of research. They can be used in the zero temperature limit and are thus playing a valuable role in the investigation of QT.

A. Oscillating grid experiments

The first attempts to generate QT by an oscillating grid and to detect it by means of ions are from McClintock's group in Lancaster,[66] using the apparatus shown schematically in the top of Figure 16. The grid is held at a high constant potential. The perforated top and bottom electrodes complete the double capacitor, and oscillations of the grid are excited by application of an alternating potential to the lower electrode, producing QT above a certain threshold (see later). A

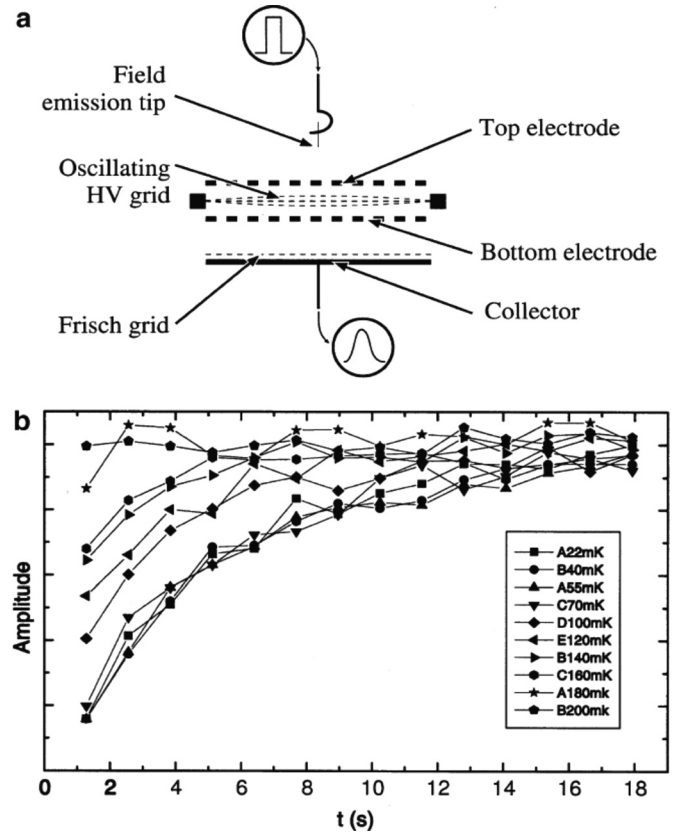

FIG. 16. Experimental arrangement (schematic) to generate QT by oscillating a tightly stretched grid and for measuring its decay times (a). Evolution of the collector signal with time following a burst of grid oscillations[66] (b).

sequence of ion pulses is then generated by the field emission tip. Some ions from each pulse get trapped on vortices, thereby reducing the signal arriving at the collector.

The bottom section of Figure 16 plots the evolution of the collector signal with time following a burst of grid oscillations, for different temperatures. It is evident that the recovery of the signal amplitude to its vortex-free level takes several seconds, attributable to the time taken for QT to decay. This illuminating experiment clearly demonstrated the production and decay of QT in the zero temperature limit, although only qualitatively.

An experimental setup based on the electromagnetically towed grid ^{4}He that ought to work at very low temperatures is under development in Florida by Ihas *et al.*[67]; however, only preliminary qualitative data based on calorimetric technique (i.e., monitoring the temporal rise of the temperature of the working fluid after pulling the grid though a stationary sample of He II) are available at present.

It is important to note that QT has been quantitatively investigated in superfluid ^{4}He and in fermionic superfluid ^{3}He-B. In the latter, QT is possible at low enough temperature only[68] (see later) because of the very high viscosity of the normal fluid and strongly temperature dependent mutual friction force. Much useful information has been obtained using the nuclear magnetic resonance technique,[69] but in this section we shall be concerned with the data in the zero temperature limit, where the Lancaster ^{3}He group invented a new experimental technique based on Andreev scattering of quasiparticles caused by the velocity field of quantized vortices.

The experimental arrangement for the first vibrating grid experiments[70] in ^{3}He-B at low temperatures, achieved using the Lancaster style nuclear cooling stage,[71] is shown in Figure 17. The grid is made from a fine mesh of fine copper wires spaced 50 μm apart, leaving 40 μm square holes. Facing the grid are two vibrating wire resonators made from 2.5 mm diameter loops of 4.5 μm NbTi wire, positioned 1 mm and 2 mm from the grid, respectively. An additional wire resonator (not shown in Figure 17) is used as a background thermometer.

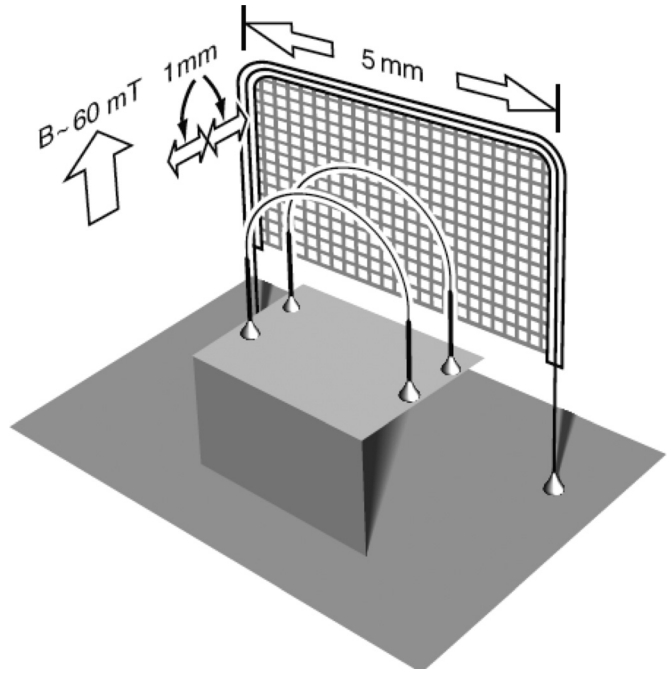

FIG. 17. Experimental arrangement of the oscillating grid in ^{3}He-B and associated vorticity detector wires.

The underlying physics of Andreev scattering detection technique is explained in the review by Fisher and Pickett.[72] Briefly, the equilibrium number of quasiparticles (and quasiholes, as ^{3}He-B is a fermionic superfluid) can be sensed by a vibrating wire resonator. The drag force exerted by these quasiparticles is reduced if the vibrating wire is surrounded by QT, as some of incoming quasiparticles (quasiholes) cannot reach it, being Andreev reflected by the energy barrier of the velocity field of the superflow near the vortex core. The fractional decrease in damping can then be converted into the vortex line density in the tangle.

With this technique, using the vibration amplitude of the grid above a certain value, it was possible[73] to observe the transition to QT. While the detailed processes are no doubt complex, the current view is that the vibrating grid emits vortex rings more frequently with increasing grid velocity. At some critical velocity the density of rings becomes sufficiently high that they can no longer avoid each other. Subsequent reconnection brings more complex shapes and a cascade of further reconnections leading rapidly to QT. This scenario, backed by the Osaka Tsubota's group computer simulations of Fujiyama *et al.*,[74] is illustrated schematically in Figure 18.

The Andreev scattering technique allowed investigations of the decay of vortex line density in ^{3}He-B in the zero temperature limit.[75] The results are shown in Figure 19 together with the data from Oregon towed grid experiment in He II at $T = 1.3$ K. We see the striking similarity between these data sets, for decay curves in ^{3}He-B corresponding to grid vibrations above certain amplitude. The decay curves for grid amplitudes of lower magnitude display different decay curves, for most of the time roughly following the $L(t) \propto 1/t$ decay law (see the decay curves close to the theoretical decay curve D in Figure 19).

The Lancaster group recently extended these investigations in terms of fluctuations and correlations of pure quantum turbulence in ^{3}He-B in the zero temperature limit.[76] The interesting result is that the frequency power spectrum of vortex line density (not energy!) displays, for high amplitude of the grid vibration, i.e., for very intense quantum turbulence, a $-5/3$ power law behavior. Note in passing that similar results were obtained also in He II, by Roche *et al.*[77] and explained by Roche and Barenghi.[78] They argue that the disagreement is solved if the vortex line density field is decomposed into a polarised field (which carries most of the energy) and an isotropic field (which is responsible for the spectrum).

In the most recent Lancaster ^{3}He-B experiment with the oscillating grid,[79] Bradley and coworkers succeeded to directly measure the energy decay rate ϵ in the zero temperature limit,

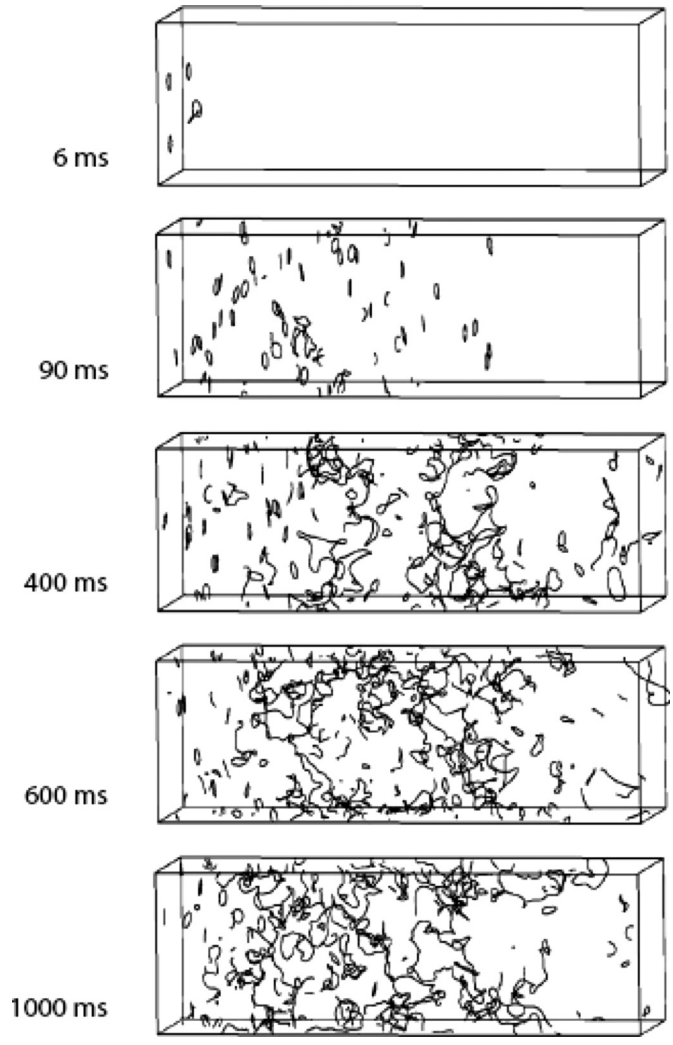

FIG. 18. Simulation of quantum turbulence formation due to oscillating grid.[74] Each frame shows the vortex configuration at the labeled time. Rings injected from the left quickly collide and recombine producing a vortex tangle which evolves on longer time scales.

inside a box acting as a black body radiator of quasiparticles. This experiment can be thought of as a complementary one to those described above. As we discuss later, it also might be more directly compared to decaying classical turbulence, as (although the detection technique is very different) the quantity measured—the energy decay rate—is the same.

B. QT in spin-down experiments

We shall particularly discuss the Manchester data in the zero temperature limit, obtained in the spin down experiments in He II by Golov, Walmsley, and coauthors, who introduced an improved technique based on negative ions.[69,80–82] Negative ions (electron bubbles) are injected by a sharp field-emission tip and manipulated by applied electric field. At $T > 0.8\,\mathrm{K}$ bare ions dominate, at $T < 0.7\,\mathrm{K}$ these ions are self-trapped on the core of a quantized vortex rings of diameter about 1 μm. Short pulses of these probes are sent across the experimental container. The relative reduction in their amplitude at the collector, due to the interaction of charged vortex rings with vortex tangle in the container, is converted into vortex line density. An accurate *in-situ* calibration is possible, as these experiments have been conducted on the rotating cryostat in which a known density of rectilinear vortex lines can be created.

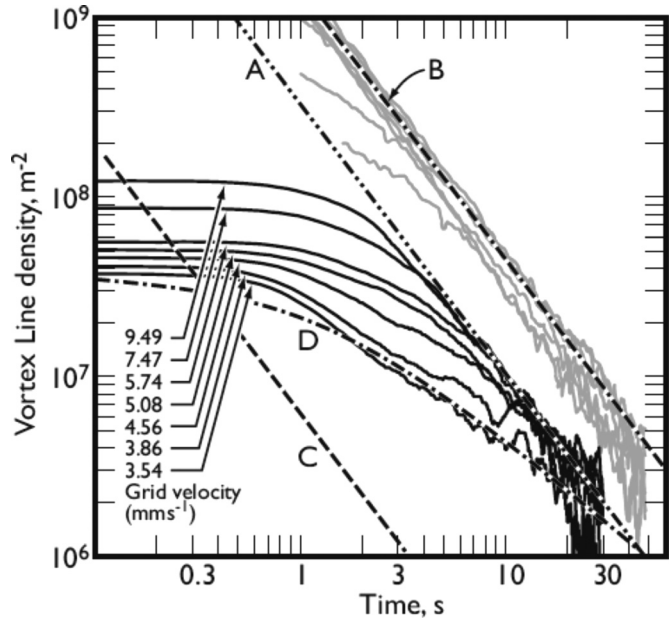

FIG. 19. Solid black curves show the inferred vortex line density as a function of time after the cessation of grid motion for initial grid velocities as indicated. Line A is the limiting classical-like behavior as discussed in the text. The halftone data is that for the Oregon towed grid experiments of Skrbek, Niemela, and Donnelly[58] in He II, with line B showing the late-time limiting behavior. Line C shows the expected behavior for the data assuming the classical dissipation law in thick normal ^{3}He. Curve D shows the expected (based on Vinen's equation, as discussed above) behavior for a random tangle in superfluid ^{3}He.[75]

We focus first on the impulsive spin-down technique, which proved suitable for temperatures down to at least 80 mK. Its success relied on rapidly bringing to rest a rotating cubic-shaped container (see upper part of Figure 20) of He II, 4.5 cm in size.[80] The range of angular velocities of initial rotation was 0.05-1.5 rad/s. In order to probe the vortex densities along the axial and transverse directions, there were two independent pairs of injectors and collectors of electrons. Both

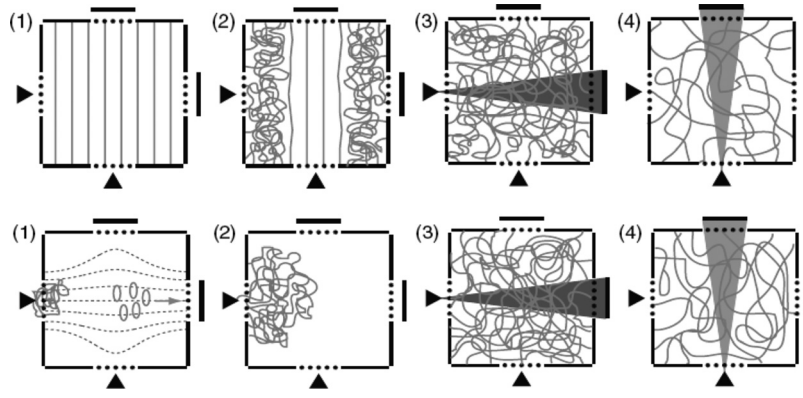

FIG. 20. Upper row: Cartoon of the vortex configurations produced by spin-down in the experimental cell (side view) at different stages. (1) Regular array of vortex lines during steady rotation before deceleration. (2) Immediately after stopping rotation, turbulence appears at the outer edges but not on the axis of rotation. (3) After about 30 rad of initial rotation, the 3D homogeneous turbulence is everywhere and (4) decays with time. Shaded areas indicate paths of probe ions when sampling the vortex density in the transverse (3) and axial (4) directions. Bottom row: Cartoon of the vortex configurations produced by a pulse of injected ions at $T < 0.5$ K in the experimental cell (side view) at different stages. (1) up to 1 s: a pulse of charged vortex rings is injected from the left injector. While most make it to the collector as a sharp pulse, some get entangled near the injector. (2) $\simeq$ 5 s: the tangle spreads into the middle of the cell. (3) $\simeq$ 20 s: the tangle has occupied all volume; from now on, it is nearly homogeneous (as probed in two directions). (4) Up to 1000 s: the homogeneous tangle is decaying further. The shaded areas indicate the trajectories of ions used to probe the tangle along two orthogonal directions.

injectors and collectors were protected by electrostatic grids. The injectors were sharp field emission tips made of tungsten wire. The top, bottom, left, and right electrodes had circular grids in their centers. All grids were made of square tungsten mesh with geometrical transparency of 92%. Further details can be found in Ref. 82.

Before making each measurement, the cryostat was kept at steady rotation for at least 300 s before decelerating to a stop; data were taken after waiting for a time interval t. Then the probed tangle was discarded and a new one generated. Hence, different data points represent different realizations. The deceleration was linear in time taking 2.5 s for $\Omega = 1.5$ rad/s and 0.1 s for $\Omega = 0.05$ rad/s. The origin of time was chosen at the start of the deceleration.

An example of the deduced transverse vortex line density and its time development is shown in Figure 21. It is a common feature of the data (measured along both horizontal and vertical direction at any temperature) that after certain transient the vortex line density decays as $L(t) \propto t^{-3/2}$. To stress the scaling of the characteristic times with the initial turnover time Ω^{-1} and the universal late-time decay, the data are rescaled accordingly. At all Ω the observed transients are all basically universal. The scaling of the transient times with the turnover time Ω^{-1} indicates that transient flows are similar at different initial velocities, which is expected for flow instabilities in classical liquids. Eventually, after $\Omega t \cong 100$, the decay takes its late-time form $L(t) \propto t^{-3/2}$ expected (for vorticity, not for energy) for classical isotropic turbulence in the bounded domain. At $0.08 < T < 0.5$ K, the measured $L(t)$ were independent of temperature.

In Figure 21 the observed densities $L(t)$ at low ($T = 0.15$ K) and high ($T = 1.6$ K) temperatures are compared. It is important to mention that in the temperature range of overlap a good quantitative agreement exists with the discussed above Oregon towed grid decay data. Note that the prefactor in the late-time dependence $L(t) \propto t^{-3/2}$ at $T = 0.15$ K is almost an order of magnitude larger than that for $T = 1.6$ K. This implies that at low temperature the steady state inertial cascade with a saturated energy-containing length and constant energy flux down the range of length scales requires a much greater total vortex line density.

C. QT generated by ion jets

An alternative technique of generating turbulence by a jet of injected ions, requiring no moving parts in the cryostat, has been developed by Walmsley and Golov.[80–82] The generation and detection method is illustrated in the bottom part of Figure 20. The authors found that the properties of these tangles can be quite different. This difference is most clearly demonstrated while observing their temporal decay rates. Figure 22 confirms that two distinctly different power law decays are observed, depending on experimental conditions. Basically, instances of QT produced after short injection of ions at low temperatures display $L(t) \propto t^{-1}$ decay, while those

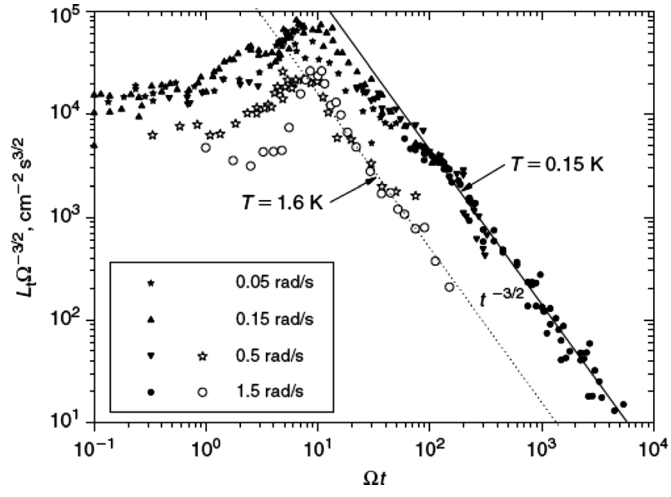

FIG. 21. Deduced vortex line density, normalized, for $T = 0.15$ K (filled symbols) and $T = 1.6$ K (open symbols). Dashed and solid lines have a slope of $-3/2$ to guide the eye through the late-time decay at $T = 1.6$ K and 0.15 K, respectively.

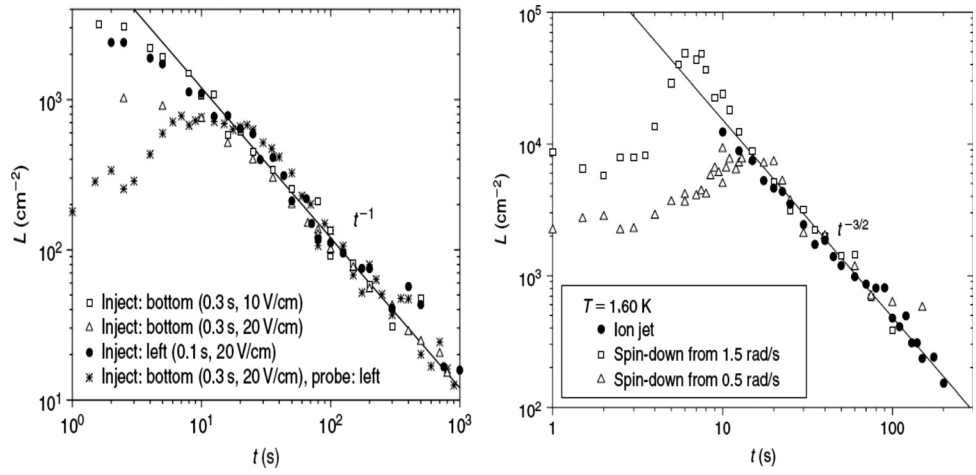

FIG. 22. Left: Temporal decay of a tangle produced by beams of charged vortex rings of different durations and densities at $T = 0.15$ K. The injection direction and duration and driving fields are indicated. Right: Decay of a tangle produced by a jet of free ions from the bottom injector (•), as well as by an impulsive spin-down to rest from 1.5 rad/s and 0.5 rad/s. All tangles were probed by pulses of free ions in the horizontal direction.

generated after long injection at high temperatures display $L(t) \propto t^{-3/2}$ decay law, in agreement with quantum turbulence generated by rapid spin-down technique. At temperatures 0.7–1.6 K, the late-time decays of vortex line density generated by these two different techniques were identical within experimental error.

Note in passing that the ion jets generation method creates charged vortex tangles, which opens new possibilities to study quantum turbulence with additional interesting properties. For example, Coulomb repulsion among charged ions trapped on cores of quantized vortices affects the dynamics of the vortex tangle; further charging of an existing tangle might lead to its polarization, etc. These questions are, however, beyond the scope of our review and we direct the interested reader to the recent original publication of Golov, Walmsley, and Tompsett.[83]

VII. QT IN A STATIONARY NORMAL FLUID

We consider QT in superfluid phase ^{3}He-B at relatively "high" temperatures (i.e., in terms of T/T_c, where the superfluid transition temperature T_c depends on pressure and is of order 1 mK), where its flow can be described by the two-fluid model. The kinematic viscosity of the normal fluid in ^{3}He-B is high enough that in experimental containers of typical size of 1 cm^3 the normal fluid hardly moves and a completely new class of QT becomes possible when only the superfluid component is moving with respect to boundaries. The situation is essentially different from He II where the normal fluid possesses very low kinematic viscosity and may easily become turbulent. The relevant experiments have been carried out by the Helsinki ROTA group using the rotating cryostat that has contributed over many years to our knowledge on rotating superfluid ^{3}He phases.

A. NMR experiments on QT in ^{3}He-B

The experiment is basically organized as follows: The ^{3}He sample is contained inside a long ($\approx$11 cm) quartz tube of $2R = 6$ mm in diameter with smooth walls, connected only via a small orifice in the bottom to the heat exchanger volume on the nuclear demagnetization stage of the rotating cryostat. Three independent superconducting coils produce axially oriented magnetic fields, at both ends of the tube (for the NMR measurements), as well as in the middle, this being called the barrier field serving to stabilize the superfluid ^{3}He A-phase in this part of the sample. For a wide range of pressures and temperatures this geometry allows stabilizing the A/B boundary in the cell.

In rotating ^{3}He-B the critical velocity for intrinsic vortex nucleation is rather high and vortex-free superflow (the so-called Landau state) can be maintained up to high angular velocities. Other metastable states with intermediate number of rectilinear vortex lines, up to the equilibrium

number N_{eq}, are also stable. On the other hand, the critical velocity for vortex nucleation in the floating above A-phase is low and can be neglected for our purposes here. Therefore the rotating A-phase can always be thought of as containing (nearly) equilibrium number of vortices mimicking its solid body rotation. If the cryostat is slowly accelerated from zero up to some angular rotation velocity Ω, the following configuration is possible: below the stable A/B boundary the B-phase is in the vortex-free Landau state while above it the A-phase is in solid body rotation. Note that in both phases, the normal fluid always rotates together with the container, providing a unique frame of reference.

It has been shown by Blaauwgeers *et al.*[84] that at some critical angular velocity Ω_{cr} the A/B boundary undergoes the shear wave Kelvin-Helmholtz instability and injection of few vortices from the A-phase to the B-phase occurs. This is the mechanism by which in the experiment ΔN "seed" vortex loops are introduced into the B-phase, which is otherwise in the vortex-free Landau state.

As schematically shown in Figure 23, the outcome of this injection falls in one of two categories. At high temperature the final number of vortices found after some time in the B-phase, N_f, equals the number of injected ones, ΔN. It takes some transition time, typically a few seconds, until the injected "seeds" expand and form a rectilinear array in the vicinity of the rotation axis. At low temperature, however, turbulent loop expansion occurs and $\Delta N \ll N_f \leq N_{eq}$. This process leads to a total removal of the macroscopic vortex-free superflow as the superfluid component is

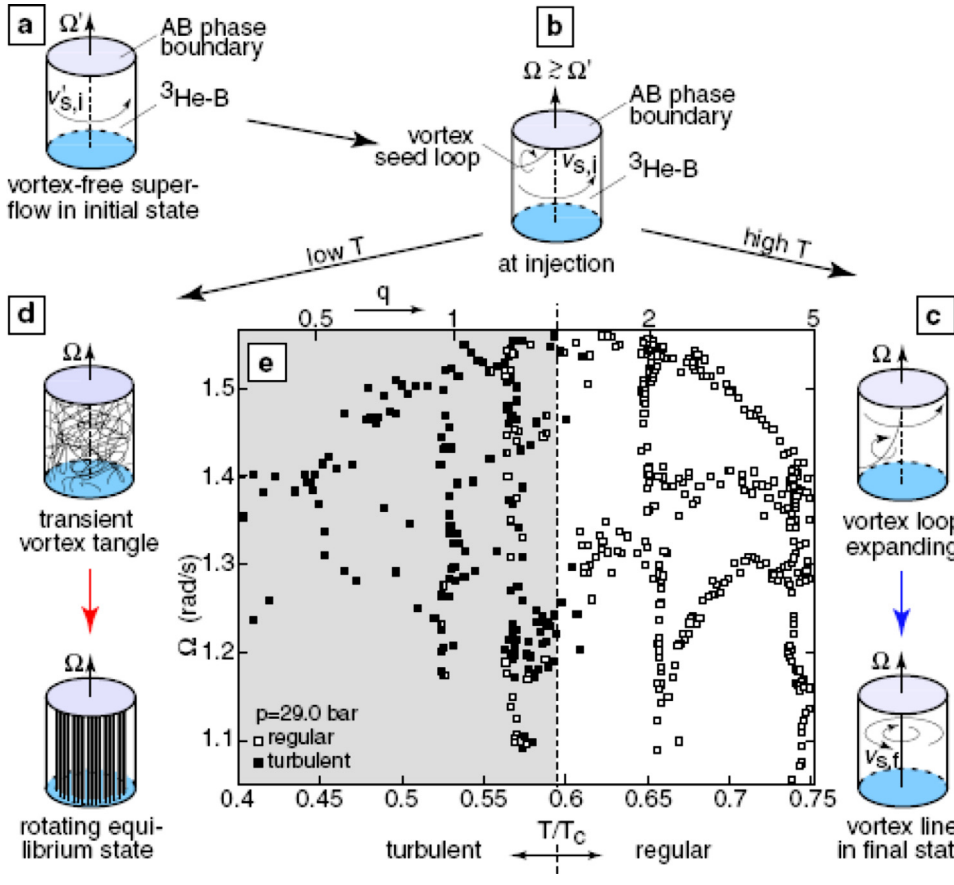

FIG. 23. (Color online) Phase diagram of turbulent superflow in ^{3}He-B found by Finne *et al.*[68] The principle of the measurements is as follows. (a) The initial state is vortex-free (Landau state) superflow in rotation at Ω, where the normal component is stationary and the superfluid component flows in the rotating frame. (b) A few (ΔN) vortex loops are injected and, after a transient period of loop expansion, the number of rectilinear vortex lines N_f in the final steady state is measured. This state is found to fall in one of two categories. (c) $N_f = \Delta N$, regular mutual-friction-damped loop expansion. (d) $\Delta N \ll N_f \leq N_{eq}$, turbulent loop expansion. This process leads to a total removal of the macroscopic vortex-free superflow as the superfluid component is forced into solid-body-like rotation (on an average) by the formation of a vortex array with the equilibrium number of rectilinear lines, $N_{eq} \approx \pi R^2 2\Omega/\kappa \sim 10^3$. (e) Phase diagram of measured events.

forced into solid-body-like rotation (on an average) by the formation of a vortex array with the equilibrium number of rectilinear lines, $N_{eq} \approx \pi R^2 2\Omega/\kappa \sim 10^3$. Figure 23 also shows the experimentally observed phase diagram of turbulent superflow in ^{3}He-B. Each data point monitors the outcome from the injection event in the final steady state as a function of rotation and temperature. Regular loop expansion is marked with open symbols and the turbulent state with filled ones. An abrupt transition at 0.60 T_c, independently of Ω, has been found to divide the (Ω, T) plane vertically into the two types of vortex dynamics. Only within a narrow interval $\Delta T \approx 0.05\ T_c$ around 0.60 T_c can the intermediate behaviour be observed.

Figure 24 shows how the authors of Ref. 68 came to the above conclusions based on the observed NMR spectra. NMR in ^{3}He-B does not directly measure the number of vortices in rotation, but the spectral shape reflects the spatial texture of the sample. The texture problem consists of finding the spatial distribution of the rotation axis $\hat{\boldsymbol{n}}$ of the order parameter. The overall NMR absorption signal from the sample can be thought of as consisting of the signal of a number of small volumes (local oscillators) of constant angle β between $\hat{\boldsymbol{n}}$ and magnetic field direction. The normalized frequency shift from the Larmor frequency for each of these oscillators is approximately proportional to $\sin^2\beta$. Hence the overall shape of the observed NMR spectrum depends on the texture. The type of the texture is a result of interplay of orienting interactions among the magnetic field energy, the flow energy, and the surface energy.

It is known that in a long cylindrical sample at rest the so called flare-out texture establishes: $\hat{n}$ points up at the rotation axis of the container (i.e., $\beta(0) = 0$), off the axis it bends out and reaches an angle $\beta(R) \approx 63$ degrees at the wall. The influence of rotation on the texture in a cylindrical container is rather complicated (there are several textural transitions induced by rotation—see the original work[85])—but the observed NMR spectra shown in Figure 24 can be interpreted as follows:

The two spectra on the left, marked (a), represent the vortex-free Landau state and its only minor changes introduced by regular mutual-friction-damped loop expansion above 0.60 T_c. The sharp peak at large frequency shift (from the Larmor frequency) is caused by the large-scale superflow present in the rotating frame. When a few rectilinear vortex lines are formed, some absorption from the large peak is shifted into a tiny new peak at small frequency shift. The heights of both peaks change approximately linearly with N_f (in the highlighted regions).

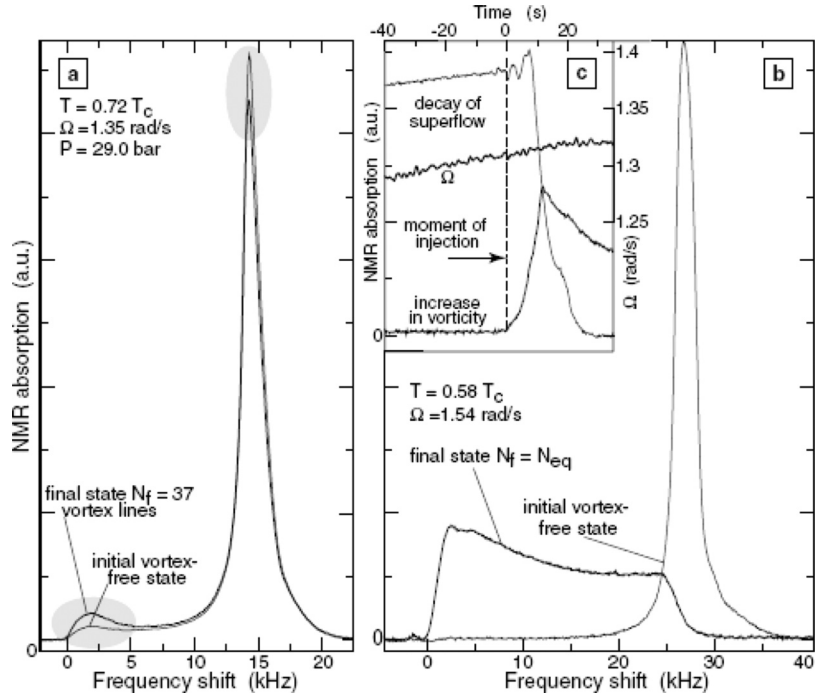

FIG. 24. NMR absorption spectra before and after vortex-loop injection[68] (see text for details).

The two spectra on the right, marked (b), show a radical restructuring that occurs below 0.60 T_c when the large-scale superflow is replaced by an equilibrium array of rectilinear vortices.

The inset (c) displays peak heights of the two absorption maxima as a function of time during the transient turbulent period: (i) The sharp peak at large frequency shift decreases, monitoring the decay of the large-scale superflow. (ii) The tiny peak at small frequency shift first increases, reflecting the build up of the high-density vortex tangle. Subsequently it starts to decrease, corresponding to the rarefaction and polarization of the tangle into an equilibrium array.

The Helsinki data clearly show that the transition between regular high-temperature processes (marked with open symbols in the phase diagram in Figure 23) and turbulent low temperature processes (filled symbols) observed at 0.60 T_c is surprisingly sharp, with $N_f \sim 1$ above and $N_f \approx 10^3$ below the transition. The main conclusion is that the transition occurs as a function of temperature, with little or no dependence on the maximum superflow velocity $U = \Omega R$, in striking contrast to the situation in classical liquids.

By injection of vortex loops into a sample of ^{3}He-B in the Landau state (i.e., the thick normal fluid rotating with the container; the superfluid at rest, no vortices) an interesting twisted vortex bundle becomes generated.[86] Careful experimental studies on the Helsinki ROTA group show that a vortex front propagating into a region of vortex-free ^{3}He-B changes its nature from laminar, via quasiclassical turbulent, to quantum turbulent with decreasing temperature and provide direct measurement of the dissipation rate in turbulent vortex dynamics.[87]

VIII. DISCUSSION OF THE PHENOMENOLOGICAL THEORY OF QT

A. Classical turbulence versus quantum turbulence

A main aim of this article is to pay attention to common features and differences between classical and quantum turbulence. For this purpose, we have described in some detail a number of experiments in both He II and ^{3}He-B where QT has been generated and detected in various ways. We have provided a number of experimental details for the benefit of the discerning reader.

Except for the Maurer and Tabeling experiment[6] with counterflowing discs and very recent experiments of Salort *et al.*[49] (providing information of the energy spectral density) nearly all other experiments measure vortex line density, L, especially its temporal development $L(t)$, in decaying QT. We stress that the quantitative $L(t)$ data display identical (or at least very similar) features in all cases, although they have been obtained in both bosonic (He II) and fermionic (^{3}He B) superfluids using very different experimental methods (second sound attenuation, Andreev reflection, ion and ion-vortex rings propagation, etc.). This fact strongly suggests that the conclusions have some credibility to them.

We have seen that the decaying vortex line density observed in various experiments can be divided roughly into two categories: $L(t) \propto t^{-1}$ and $L(t) \propto t^{-3/2}$. We shall argue that these two categories of quantum turbulence, which are sometimes called as Vinen and Kolmogorov quantum turbulence, can be described and their main features understood, on the basis of simple consideration of their 3D energy spectra.

B. General shape of the 3D energy spectra in classical turbulence and QT

The shape of the 3D energy spectrum for 3D turbulence in classical viscous fluids is reasonably well known for the homogeneous and isotropic case. Neglecting intermittency corrections, it follows from Kolmogorov's dimensional reasoning that, for high enough Reynolds number, an inertial range of scales ℓ exists, where the spectral energy density takes the form,

$$\phi(k) = C\epsilon^{2/3}k^{-5/3}. \tag{29}$$

Here k is the wavenumber, $\epsilon = -dE/dt$ denotes the energy decay rate and C is the 3D Kolmogorov constant. On the low k end, the spectrum is naturally truncated by the size of the container $k_D = 2\pi/D$, reflecting a simple fact that eddies larger than the system, D, cannot exist. The low k end (due to the equi-partition theorem) takes the form Ak^m. We shall discuss the value of the exponent m later. On increasing k, there is a broad maximum in $\phi(k)$ that corresponds to energy

containing eddies. At scales around ℓ_e most of the turbulent energy resides. In steady-state 3D turbulence, the flow energy is injected at the outer scale $\approx \ell_e$ and, by the Richardson cascade, transmitted essentially without loss in k-space to the dissipation wavenumber, and becomes dissipated by the viscosity at $k_{\rm diss} \approx (\epsilon/\nu^3)^{1/4}$, where ν denotes the kinematic viscosity. The dissipation scale is again determined by simple dimensional reasoning.

Let us consider the simplest case of QT, the zero temperature limit where there is no normal fluid, and QT consists of a tangle of quantized vortex line. The superflow exists down to smallest length scale, which is the size of the vortex core ξ. There is no viscosity, so the notion of dissipation length scale does not apply. It is common to introduce another physical length scale defined by the mean intervortex distance that could be estimated as $\ell_v \approx 1/\sqrt{L}$. We believe, however, that from the point of view of fluid dynamics, it seems sensible to introduce a characteristic quantum wavenumber, $k_Q \approx (\epsilon/\kappa^3)^{1/4}$, and corresponding quantum length scale $\ell_Q = 2\pi/k_Q$.[88] As mentioned in the Introduction, vorticity of the superfluid component is quantized in terms of the circulation quantum $\kappa = 2\pi\hbar/M$ where M is the mass of a superfluid particle. In analogy with classical viscous flow, the flow of the superfluid component can be characterized by the "superfluid Reynolds number" $Re_s = \ell v/\kappa$. The Feynman criterion $Re_s \sim 1$ gives the velocity at which it becomes energetically favorable to form a quantized vortex—although it does not mean, due to nucleation barrier, that vortices are always created upon exceeding this criterion. The limit $Re_s \gg 1$ is equivalent to a vanishing Planck's constant, $\kappa \propto \hbar \to 0$, so that the vorticity becomes a continuous variable, as in the classical case. The very existence of the quantum length scale is thus a purely quantum mechanical effect.

The quantum length scale defined above has a clear physical meaning. It qualitatively divides the scales in quantum turbulence into large scales—where quantum restrictions in the form of quantization of circulation does not play any role (or, in other words, the "granularity" of QT does not matter)—and small scales, where quantum restrictions are essential. Beyond k_Q the spectral energy density ought to depend, in addition to $\epsilon = -dE/dt$ and k, also on κ. Dimensional argument similar to that of Kolmogorov[9] requires the spectral density in the wave-number space k to take the general form,

$$\phi(k) = C\epsilon^{2/3}k^{-5/3}f\left(\frac{\epsilon}{k^4\kappa^3}\right) = C\epsilon^{2/3}k^{-5/3}f\left(\frac{k}{k_Q}\right). \tag{30}$$

We now make the following remarks with respect to the zero temperature limit experiments described above.

In all these experiments, the quantum length scale plays the essential role of separating the Kolmogorov QT from the Vinen QT. In the case of Kolmogorov QT, the outer scale is larger than $\ell_{\rm Q}$ and the three-dimensional energy spectrum has the general form of Fig. 25. In the Vinen QT, on the other hand, $\ell_{\rm Q}$ is larger than the scale at which energy is injected into the system. Thus the quasiclassical cascade (and the Kolmogorov inertial range) cannot exist. The Vinen QT possesses quantum effects at all scales; neither stretching nor advection takes place, as the vortex tangle is random with no large eddies. Thus it has no counterpart in classical turbulence.

The quantum length scale determines the crossover from the Vinen to Kolmogorov QT. We can illustrate this crossover using the Lancaster experimental decay data obtained with the oscillating grid in the zero temperature limit in ^{3}He-B.[75] The steady state from which the decay originates is generated by the same oscillating grid, so the scale at which the quantum flow is forced is undoubtedly the same. By increasing the oscillation amplitude of the grid, more and more energy is supplied to the flow, and all this energy is being dissipated in the steady state. It is true that the turbulence generated in this way is not homogeneous and isotropic, but, at least qualitatively, increasing the oscillating amplitude of the grid results in higher rate of energy decay, ϵ and, consequently, the quantum wavenumber $k_Q \propto \epsilon^{1/4}$ increases. The crossover separating the decay in the form $L(t) \propto t^{-1}$ to $L(t) \propto t^{-3/2}$ corresponds to a grid velocity $\simeq 5\,$mm/s, when the grid is forced by $\simeq 0.2\,\mu$N.[70] Multiplying these values gives the absolute energy decay rate in the stationary case, due to decaying QT some distance from the grid. Knowing its size, we estimate the decay volume of order 5×10^{-8} m^3. The density of ^{3}He is about $100\,$kg/m^3, so this gives $\epsilon \approx 2 \times 10^{-4}\,$m^2/s^3. With known circulation quantum in ^{3}He-B $\kappa \cong 0.066\,$mm^2/s this results in $k_Q \approx (\epsilon/\kappa)^{1/4} \approx 30000\,$1/m and $\ell_{\rm Q}$ is close to the mesh size of the grid, $50\,\mu$m.

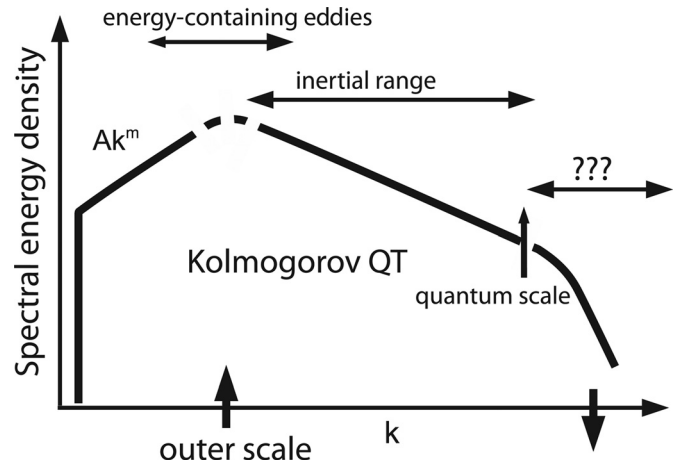

FIG. 25. The general shape of the 3D energy spectrum of QT in the zero temperature limit. For length scales exceeding the quantum length scale (to the left of the thinner vertical arrow), quantum effects are unimportant and a classical Richardson cascade operates, resulting in the inertial range of the Kolmogorov form. At smaller length scales, quantum effects start to dominate and Kelvin-waves cascade transfers energy that eventually becomes dissipated, most likely by acoustic emission (for further details, see text).

Moreover, the crossover is fully consistent with the most recent Lancaster ^{3}He-B experiment, measuring directly the energy decay rate ϵ inside a box acting as a black body radiator of quasiparticles, displaying at late time a crossover from Vinen QT $\epsilon \propto t^{-2}$ to Kolmogorov QT $\epsilon = \nu_{\rm eff}\kappa^2 L^2 \propto t^{-3}$.[79]

We believe that the Manchester experiments where QT is generated by ion jets serves as another example for a crossover from the Vinen regime (at low temperatures, where dissipation is low) to the Kolmogorov regime (where dissipation is much higher, due to the mutual friction force exerted on the tangle), with the quantum scale crossing the energy containing length scale with increasing temperature.

If indeed the 3D energy spectrum for Kolmogorov QT *in the zero temperature limit* has the $-5/3$ form as described, it would not be difficult to explain the experimental results described earlier. The existence of the inertial range accompanying the Richardson quasiclassical cascade is possible only if reconnections of quantized vortices are allowed, which, in contrast with Euler fluids, do take place in He II.[22,89] Computer simulations show that reconnections are accompanied by emissions of sound waves of wavelength of the order of the healing length.[90,91] As shown numerically by Barenghi *et al.*,[92] sound waves are emitted even in the absence of reconnections—it is sufficient that a vortex accelerates due to the presence of other vortices.

The Kolmogorov cascade cannot proceed beyond k_Q. On the other hand, there is no dissipation mechanism (except vortex reconnections, but the current understanding[40] is that it may not be efficient enough) and the cascade process has to continue towards higher k and take a form of Kelvin wave cascade. Kelvin waves on quantized vortices with well known dispersion relation then transfer the energy towards high enough frequencies, where acoustic emission of quasiparticles is efficient enough to compensate for the forcing on the outer scale. The quasiparticles thus emitted thermalize eventually and constitute the normal fluid, thus effectively increasing the temperature. As in classical turbulence, the total destiny of the flow energy is to be converted into heat. It is currently a matter of intense discussion whether Kelvin wave cascade joins the Kolmogorov cascade smoothly (Kozik and Svistunov[93]), or some form of a bottleneck exists (L'vov, Nazarenko, and Rudenko[94]). It is our opinion that these issues are not yet theoretically settled and relevant experimental data are scarce (Eltsov *et al.*[87]) and provide at best indirect evidence for various scenarios. We therefore leave them out of further discussions.

We have already discussed experimental evidence for the inertial range of scales in QT provided by Maurer and Tabeling[6] and Salort *et al.*[49] We are not aware of any direct measurement of the energy spectrum in the zero temperature limit. There is, however, significant support that comes from computer simulations. Kolmogorov spectrum was found both in the vortex filament

model outlined in the Introduction by Araki, Tsubota, and Nemirovskii[95] and using the Gross-Pitaevski model by Nore, Abid, and Brachet[96] as well as by Kobayashi and Tsubota.[97]

The situation is more complicated at temperatures where there is significant amount of normal fluid. One has to consider energy spectra in both superfluid and normal components and take into account the mutual friction that couples the two velocity fields together (for the analytical approach, see L'vov, Nazrenko and Skrbek[98] backed up by very recent computer simulations of Tchoufag and Sagaut,[99] and for numerical simulation of two fluid cascades, see Kivotides[100] and Roche, Barenghi, and Leveque[101]). The spectral shape is thus difficult to analyze in detail, especially in case of counterflow (meant here generally as a situation when mean flows in the two components are different). Unless specified, the following considerations always assume the co-flow situation.

C. Decaying turbulence

The particular problem of interest here is the decay of turbulent energy in the absence of sustained production. This problem in classical fluids has been discussed in many reviews (e.g., Lesieur[102]) since the pioneering work of von Kármán and Howarth[103] and Kolmogorov.[104] The theoretical result of Kolmogorov is that the kinetic energy of turbulence, given by $E = \overline{u^2}/2$, where $\boldsymbol{u} = \boldsymbol{u}(\boldsymbol{r},t)$ is the velocity vector, decays as $E(t) \propto t^{-\gamma}$, with $\gamma = 10/7$. This result has been challenged many times. The experimental data display rather large variability in the decay exponent, γ; and, as discussed in Ref. 56, care must be taken when evaluating γ from experimental data, due to the strong influence of the so-called virtual origin in time. Further, as pointed out in the recent theoretical study by Yakhot,[105] the results of various numerical experiments also differ substantially, whose source could be finite-size effects or differences in initial conditions. We will discuss these aspects. In particular, we will distinguish between the following two cases: (i) the energy-containing scale, ℓ, (or integral scale ℓ_i) of turbulence is equal to the size of the apparatus, D, and stays approximately so during the decay and (ii) ℓ is small enough compared to the size of the apparatus that it grows unconstrained during decay. We shall argue that carefully planned experiments on decaying QT could shed new light on the old puzzle concerning the so-called Loitsianskii invariant.[106]

D. The basic premises of comparison between QT and HIT

The basic equation for turbulent energy decay in the classical case is

$$-\frac{dE}{dt} = \epsilon = \nu\overline{\omega^2}, \tag{31}$$

where E is the turbulence energy, ϵ is the energy dissipation rate, ω is the root-mean-square vorticity and ν is the kinematic viscosity. The energy E is the integral of the spectral density $\phi(k)$ over the wavenumber k. This relation also gives the decay rate of mean-square vorticity in HIT.

The results of decay experiments in QT are given in terms of decaying vortex line density, $L(t)$. We therefore have to discuss the role of vortex line density in QT. The simplest system in which to assess the role of quantized vortex lines is a rotating bucket of He II. As discussed in the Introduction, the normal fluid in steady rotation acts like a solid body with vorticity $\boldsymbol{\omega}_n = \text{curl}\ \boldsymbol{v}_n = 2\boldsymbol{\Omega}$, and He II is threaded with a rectilinear array of quantized vortex lines parallel to the axis of rotation. Although the superfluid vorticity is restricted to vortex lines, their areal density, n_0, evolves to match the vorticity of the fluid in solid body rotation. This results in $n_0\kappa = \kappa L = 2\Omega$. Thus on length scales larger than the inter-vortex line distance, the superfluid is also in solid body rotation, with a velocity field essentially that of the normal fluid, i.e., $\langle \boldsymbol{\omega}_s \rangle = \boldsymbol{\omega}_n$.

The role of quantized vortex lines in QT is more complex. Computer simulations (e.g., Ref. 101) show that, qualitatively as in a rotating bucket, bundles of quantized vortices align on the cores of normal fluid eddies. The superfluid vorticity is comparable to the vorticity of the normal fluid eddy and the effective fluid density is equal to the total fluid density. In a turbulent flow there will be a complex tangle of vortices evolving to minimize the difference between the two otherwise independent velocity fields. The turbulent superflow thus appears to resemble classical

flow possessing an effective kinematic viscosity $\nu_{\rm eff}$. If so, the relationship between turbulent energy dissipation rate per unit volume and the mean square vorticity should apply:

$$\epsilon = -\frac{dE}{dt} = \nu_{\rm eff}(\kappa L)^2, \tag{32}$$

i.e., vorticity would be defined as κL in full analogy with the rotating bucket. This is the key relationship whose behavior invites broad comparisons of QT with its classical counterpart.

The underlying physics of Eq. (32) has been discussed in detail by Vinen.[3,9] He argued that on length scales greater than both the average spacing between the quantized vortex lines and the scale of viscous dissipation in the normal fluid, the two fluids are likely to be coupled together by the mutual friction force and to behave as a conventional fluid. On smaller length scales account must be taken of dissipation—due to the viscosity in the normal fluid, frictional interaction between the vortex lines and the normal fluid, and the radiation of sound from vortex lines.

If Eq. (32) holds, the analysis of the experimental data on decaying vortex line density ought to be straightforward, as it allows treating superfluids as a hypothetical classical fluid possessing an effective kinematic viscosity $\nu_{\rm eff}$.

E. Decaying L(t) in QT versus decaying vorticity in HIT: Results for arbitrary energy spectrum

If the outer scale of turbulence (energy-containing length scale ℓ) is equal to the size of the system, the equations of decay can be closed and one can get explicit results for the decay. Equation (31) can be approximated as $\epsilon \approx E^{3/2}/D$. This agrees with the familiar dimensional relation[107] $\epsilon = \epsilon_0 E^{3/2}/\ell$, if ℓ is replaced by the size of the system, D. It is immediately evident that the kinetic energy decays as $E(\tau) \propto D^2/(t+t^*)^2 = D^2/\tau^2$, where t^* is the virtual origin in time that depends on the starting value of energy as well as the transient processes that might take place at the start of the decay. For decaying vorticity (at late times) this corresponds to

$$\boldsymbol{\omega}(t) \propto D/(t+t^*)^{3/2} \approx D/t^{3/2}. \tag{33}$$

We emphasize that no assumptions on the shape of the 3D energy spectrum has been necessary in coming to this conclusion; the power laws for decaying energy and vorticity readily follow from dimensional reasoning.[107]

Despite the inevitability of the above result, experimental data on decaying HIT that would confirm it convincingly are scarce (let us mention here the recent experiments of Morize and Moisy,[108] primarily aimed to PIV study of the energy decay of rotating turbulence with confinement effects which, without rotation, displays results consistent with $E \propto t^{-2}$ at long times). This is not surprising because every grid-turbulence experiment has aimed to keep the length scale small compared to the wind tunnel size. On the other hand, numerical simulations, such as those of Borue and Orszag,[109] Biferale *et al.*,[110] and especially those of Touil, Bertoglio, and Shao,[111] have this ratio closer to unity. In particular, Touil *et al.* investigated the decay of turbulence in a bounded domain without mean velocity, using direct and large-eddy simulations, as well as the eddy-damped quasi-normal Markovian closure. The effect of the finite geometry of the domain is accounted for by introducing a low wavenumber cut-off into the energy spectrum of isotropic turbulence. It is found that, once the turbulent energy-containing length scale is saturated, the root-mean-square vorticity followed a power law with $-3/2$ exponent. This yields $L(t) \propto t^{-3/2}$, just as observed in Oregon towed grid experiments (Figure 15), in the decaying data of Lancaster ^{3}He-B experiment (Figure 19), and in the Manchester spin-down (Figure 21) and ion-generated data (Figure 22).

Note further that Eq. (33) shows that data obtained in two geometrically similar channels must have the same exponent but also a prefactor that shows a *linear dependence on the size of the channel*. While there are no data in classical HIT to which this simple prediction can be compared directly, we already argued that the late part of the Prague counterflow data, clearly displaying $L(t) \propto t^{-3/2}$, could be suitable for comparison. In these experiments, two geometrically similar channels yielded with fair experimental accuracy (Figure 12) not only the power law decay

exponent, but also the *linear dependence on the size of the channel*. This is one sense in which the QT data have already started to provide new information on classical decay of HIT.

F. Temporal decay for which the shape of the energy spectra matters

If the large scale of turbulence does not saturate, the details of decay depend on the precise form of the spectral density of turbulence energy. The spectral density in decaying HIT behaves differently on different scale ranges and obeys different forms of similarity, with appropriate crossovers between them. One can then use Eq. (31) to calculate the decay in terms of the dynamics of crossover scales and other spectral constants such as scaling exponents. This procedure was first used by Comte-Bellot and Corrsin[51] and revised by Saffman[55]; it was extended in Refs. 8 and 56, while also taking account of ideas of Eyink and Thomson,[57] to develop a spectral decay model for classical HIT and to relate it to available data on decaying turbulent energy. The outcome of the model was also compared with the He II Oregon grid data on the vortex line density $L(t)$. Skrbek and Stalp[56] identified four regimes of decay, which we shall consider below.

Before doing so, one preliminary consideration is needed. The last, or the fourth, stage of decay is strongly influenced by the high k end of the energy spectra. In classical HIT—neglecting possible bottleneck effects (see, e.g., Donzis, Yeung, and Sreenivasan[112])—the spectrum falls off sharply past wavenumbers on the order of the Kolmogorov value, which can be estimated from dimensional arguments as $(\epsilon/\nu^3)^{1/4}$. In Ref. 56, the high k end of the spectrum was modeled by a sharp cutoff at an effective Kolmogorov wavenumber $k_\eta \approx \gamma(\epsilon/\nu^3)^{1/4}$, where the dimensionless parameter γ is of the order unity. It was shown that, as the dissipation length grows during the decay of classical HIT, the decay rate gradually speeds up and cannot be expressed by a simple power law for all times.

It is difficult at present to account for these fine details of the last stages of decay and to relate the classical and quantum cases precisely. The fundamental reason is that the high k parts of the energy spectra in QT and HIT are quite different in character. For the simplest case of zero temperature where there is no normal fluid, no viscosity and no mutual friction, the kinetic energy cascading down the inertial range reaches the length scale of order of the intervortex distance, where quasi-classical description ceases to hold. As we already discussed, Kolmogorov's cascades will yield beyond k_Q to the Kelvin wave cascade in some fashion. In the Kelvin cascade, waves of very high frequency are generated on individual vortex lines, eventually leading to the dissipation in the form of phonon emission at very high k. We are reluctant to discuss this issue any further here; in particular, we do not examine the relationship of the exact shape of the high k part of the QT energy spectrum on the temporal decay, or vice versa. This reluctance is mainly due to the fact that there are no relevant experimental data: neither the Lancaster ^{3}He-B grid data nor the Manchester He II spin down data display any significant late-time departures from the $-3/2$ power. The situation at finite temperature is even more complicated due to the two-fluid behaviour and the mutual friction coupling the normal fluid and the superfluid.

In our subsequent discussion we therefore neglect the effects of the finite cutoff of the spectra at high k and write it in the simple form,

$$\phi(k) = 0; \quad k < 2\pi/D, \tag{34}$$

$$\phi(k) = Ak^m; \quad 2\pi/D \le k_1(t), \tag{35}$$

$$\phi(k) = C\varepsilon^{2/3}k^{-5/3}; \quad k_2(t) \le k, \tag{36}$$

which reflects the fact that eddies larger than the size of the turbulence box cannot exist. In the vicinity of the energy containing scale $\ell_e = 2\pi/k_e(t)$, where $k_1(t) < k_e(t) < k_2(t)$, the spectral energy density displays a broad maximum whose shape does not have to be exactly specified. We shall now consider the first three stages of decay. Evaluating the total turbulent energy by integrating the 3D spectrum over all k leads to a differential equation for decaying turbulent energy; and applying $\epsilon = \nu\omega^2$ leads to a differential equation for decaying vorticity, this being the quantity of primary interest here.

G. The four stages of decay of HIT

In the early stages of decay, the spectrum retains a self-similar shape. For $D \gg \ell_e$ the first decay regime is

$$E(t + t_{vo1}) = E(\tau) \propto \tau^{-2\frac{m+1}{m+3}}; \quad \ell_e \propto \tau^{\frac{2}{m+3}}; \quad \omega \propto \tau^{-\frac{3m+5}{2m+6}}. \tag{37}$$

Here t_{vo1} is the virtual origin for time. Assuming the validity of the Saffman invariant ($m = 2$), we obtain the **first regime** for decaying energy, the original Saffman result[55]) $E \propto \tau^{-6/5}$, which yields, for vorticity, $\omega \propto \tau^{-11/10}$. On the other hand, assuming the validity of the Loitsianskii invariant[106]($m = 4$), we obtain the **first regime** for decaying energy, the original Kolmogorov result[104] $E \propto \tau^{-10/7}$, which yields, for vorticity, $\omega \propto \tau^{-17/14}$.

As the turbulence decays further and ℓ_e grows, the lowest physically significant wave number becomes closer to the broad maximum around $2\pi/\ell_e$. The low wave number part of the spectrum can no longer be approximated as Ak^m. Instead, it can be characterized by an effective power m_{eff} that decreases as the turbulence decays, such that $0 < m_{\text{eff}} < m$. Equation (37) then shows that the decay rate slows down. As ℓ_e approaches D, m_{eff} essentially vanishes to zero and we arrive at the **second regime** of the decay $\omega \propto \tau^{-5/6}$.

At the saturation time, t_{sat}, the vorticity reaches its saturation value, ω_{sat}, and the growth of ℓ_e is completed. The **universal third regime** is predicted as

$$\omega(t + t_{vo2}) = \omega(\tau) = \frac{\sqrt{27}D}{2\pi}\sqrt{\frac{C^3}{\nu}}\tau^{-3/2} \tag{38}$$

with the different virtual origin time t_{vo2}. This regime is universal in that the decaying system must sooner or later reach it, independent of the initial level of turbulence (providing it is high enough for the viscosity corrections to be negligible). In practice, since transitions from one decay regime to the next are gradual, care must be taken while searching for the decay exponent from log-log plots of the decay data, as each of the decay regime may have its own virtual origin.

As we have already anticipated, we shall not consider the fourth stage of decay.

H. Stages of decay in $L(t)$ and comparisons with HIT

The most pronounced feature of the Oregon towed grid data is that they clearly display four different decay regimes[56] that appear sequentially as the decay proceeds. We have already pointed out that the fourth stage of decay should, in fact, be different for classical HIT and QT due to the distinctive difference in the high k parts of the 3d energy spectra. As before, we focus our attention only on the other three regimes.

Focusing now on the first regime of the decay, we note that[8,56] based their work on the Oregon towed grid data and concluded that the decay exponents ($L(\tau) \propto \tau^{-11/10}$; $E(\tau) \propto \tau^{-6/5}$) are in agreement with the spectral decay model based on the validity of the Saffman invariant, which assumes that the total momentum of the flow is conserved and as a consequence the spectral energy density $\phi(k) \propto k^2$ at low k. If, however, one assumes that the angular momentum of an entire flow is conserved, then, as shown by Landau and Lifshitz,[16] this is equivalent to the validity of Loitsianskii invariant, as a consequence of which the spectral energy density $\phi(k) \propto k^4$ at low k. Even though Proudman and Reid[113] claimed that the Loitsianskii invariant is not an invariant of the motion, the issue turns out to be more complex. Recently, Yakhot[105] argued that a modified Loitsianskii integral is an invariant of the three-dimensional decaying HIT. In their recent work, Ishida, Davidson, and Kaneda[114] show that the Kolmogorov decay law $E(\tau) \propto \tau^{-7/10}$ holds numerically in a periodic domain whose dimensions are much larger than the integral scale. In view of this, we have critically re-analyzed the *Oregon* data and believe that, taking into account that the decay exponents in the first regime differ only slightly between the two cases, [($L(\tau) \propto \tau^{-11/10}$ versus $L(\tau) \propto \tau^{-17/14}$], the experimental accuracy and temporal resolution of the second sound technique does not allow firm conclusions to be drawn. As other available data on decaying

QT are certainly no better, it is our considered opinion that no conclusive experimental answer exists at present.

The second regime cannot strictly be characterized by a single decay exponent; it is more in the nature of a slow changeover corresponding to the time when the energy containing length scale is close to saturation and the broad maximum in the spectral energy density is almost flat. This slower decay regime with $L(\tau) \propto \tau^{-5/6}$ and $E(\tau) \propto \tau^{-2/3}$ does not depend on the model (e.g., on the validity of the Loitsianskii or Saffman invariant as long as there is a broad maximum in spectral energy density) and ought to occur in all experiments. It is fair to say that it indeed does exist in the Oregon towed grid data, and is at least consistent with the Manchester spin down data (see, e.g., Figure 21) and with the Lancaster ^{3}He-B data (see Figure 19). If the second regime in these data sets is displayed, it is clearly followed by the third universal regime $L(\tau) \propto \tau^{-3/2}$. It is unclear if a more careful quantitative analysis of these data sets could bring greater confidence in our reasoning, as the initial state of QT in these experiments is spatially non-uniform.

Despite this cautious conclusion, it seems that the decaying QT is capable of resolving this fundamental issue. In the Oregon experiments, the channel dimension was 1 cm and saturation of ℓ_e took place too early to observe the first regime over sufficiently long time span for extracting the power law exponent accurately enough. The conditions will probably be difficult to improve in repetitions of the same experiment. On the other hand, increasing the channel size by an order of magnitude seems experimentally feasible, and capable of answering the puzzle on Loitsianskii versus Saffman invariants. There is thus a clear call to design such an experiment on decaying QT in ^{4}He.

The third, and universal, regime concerns the $-3/2$ roll-off which we have already seen to be ubiquitous as soon as the length scale ceases to grow in time.

I. Effective kinematic viscosity

Assuming that the K41 form of the QT energy spectra holds at all temperatures over length scales up to $\ell = D$, the classical decay model[8,56,58] predicts for the decaying L not only the $-3/2$ power law but also the prefactor,

$$\kappa L(t) = \frac{D(3C)^{3/2}}{2\pi\sqrt{\nu_{\rm eff}}}(t + t_{vo})^{-3/2} \cong \frac{D(3C)^{3/2}}{2\pi\sqrt{\nu_{\rm eff}}}t^{-3/2}. \tag{39}$$

Having verified that $L \propto D$, we can describe the decaying QT in quasi-classical manner by introducing the effective kinematic viscosity, $\nu_{\rm eff}(T)$. At the same time this quasiclassical description of QT makes sense if, and only if, values of $\nu_{\rm eff}(T)$ deduced from various data sets (especially among those measured by different techniques) agree with each other. So far this check has been possible only for QT in He II.

The first attempt to extract the temperature dependence of $\nu_{\rm eff}(T)$ was done by Stalp *et al.*[59] based on the original Oregon data set, later refined by Niemela, Sreenivasan, and Donnelly[60] and Niemela and Sreenivasan[14] by adding the refined Oregon data set, obtained with the towed grid of improved design. Chagovets, Gordeev, and Skrbek[115] pointed out some corrections to these values of $\nu_{\rm eff}(T)$ and added the values $\nu_{\rm eff}^{\rm cf}(T)$ determined from the Prague counterflow data. Golov *et al.*[80–82] added their values of $\nu_{\rm eff}(T)$, deduced from the Manchester spin down and ion-injection data, where $L(t)$ was determined by using bare ions and charged ion rings. All these data are plotted in Figure 26 (note in passing that this procedure cannot be applied with any confidence for the decaying ^{3}He-B data, as D is not known).

In the overlapping temperature region all these sets of $\nu_{\rm eff}(T)$ agree with each other within the experimental scatter. Moreover, recently Chagovets and Skrbek[116,117] deduced additional set of $\nu_{\rm eff}(T)$, based on Prague superflow experiments in channels covered by superleaks in such a way that only superflow through the channel is possible. Although these data are deduced from the decay of the exponential form (for details, see recent papers[116,117]), their data also agree with the previous sets. We believe therefore that, provided that conditions allow coupling of the normal and superfluid eddies (co-flow turbulence), such a quasi-classical description of turbulent He II is

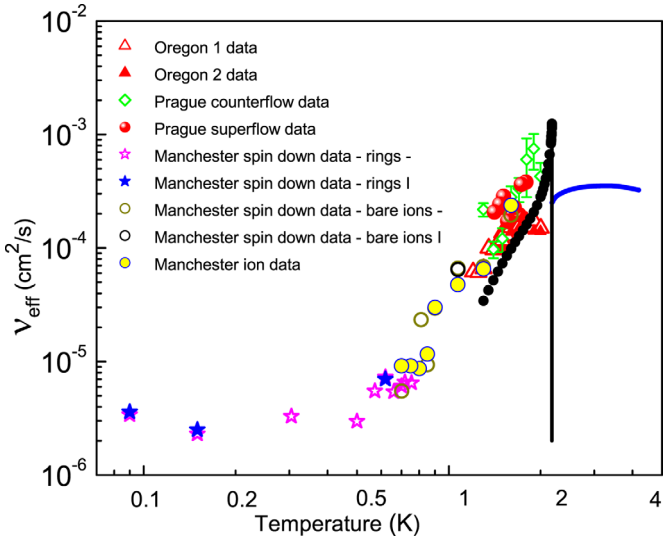

FIG. 26. (Color online) The observed temperature dependence of $\nu_{\rm eff}(T)$ from various experiments described in the text. The solid (blue) line above the λ-temperature is kinematic viscosity of normal liquid He I.[10] The big black dots correspond to our estimate $\nu_{\rm eff} \approx \kappa q$, as described in the text.

physically sound and opens possibilities of using He II as a working fluid with truly remarkable physical properties for applied fluid dynamics.

J. Alternative approach to decaying inhomogeneous QT

In case of inhomogeneous QT, or when the turbulent vortex tangle does not fill the experimental space fully (which is usually the case when QT is generated by some oscillating structure) and exists rather in a form of a packet of quantized vorticity, one has to consider another possible decay mechanism called by Barenghi and Samuels[118] as evaporation of a packet of quantized vorticity, or sometimes simply quantum evaporation. The physical principle is that during reconnections in the tangle a gas of small vortex loops is created and those of suitable orientation fly away from the tangle carrying energy and momentum with them. It can be thought of as a peculiar form of diffusion in an inviscid fluid. To illustrate that, we use the instructive work of Tsubota, Araki, and Vinen.[119] They numerically grow a dense tangle of quantized vortex line due to counterflow of normal and superfluid component, then remove one half of the tangle from the right hand side of the experimental cube, reduce the temperature to zero (i.e., remove the normal fluid and counterflow that was needed to create the tangle) and consider its development in time and space. They found that the quantized vorticity expands into the empty space in accord with the 1D diffusion equation of the form,

$$\frac{dL}{dt} = -\chi_2 \frac{\kappa}{2\pi} L^2 + D_d \nabla^2 L, \tag{40}$$

where χ_2 is an adjustable parameter and D_d denotes the diffusion coefficient. It is easy to see that this equation is directly related to the Vinen equation (18) for $v_{ns} = 0$ and $g(0) = 0$ that, as we already discussed, predicts the inverse time decay for the vortex line density $L(t) \propto 1/t$ at long times, a pronounced signature of Vinen QT. The added diffusion term in Eq. (40) generalizes the temporal decay of Vinen QT by taking into account inhomogeneity of the initial vortex tangle.

It seems clear therefore that the vortex line density of inhomogeneous tangle both decays in time and diffuses away. It is possible to estimate the magnitude of the RHS terms in Eq. (40). Following,[119] one can argue that the only relevant length scale is $\ell_v = 1/\sqrt{L}$ and the only relevant velocity scale is of order κ/ℓ_v. It follows that D_d must be of order κ (as it was indeed observed in Ref. 119) and the numerical prefactors in RHS of Eq. (40) are thus of the same order.

It is interesting to estimate the possible role of the quantum evaporation mechanism in the observed decay in the zero temperature limit Lancaster experiment,[75] where the tangle was created

by an oscillating grid in ^{3}He-B. It seems conservative estimate for inhomogeneity to assume that the vortex line density does not vanish faster than over the energy containing length scale; thus the diffusive term is of order $\kappa\nabla^2 L \approx \kappa L/\ell_e^2$. The observed classical decay of the form $L(t) \propto t^{-3/2}$ indicates that the energy containing length scale is saturated and equal to the distance of the sensor (vibrating wire) from the grid, i.e., of order 1 mm. This estimate may not seem to be correct from the point of view that it is not *a priori* known that we deal with the Kolmogorov QT, but to estimate the gradient based on the distance between the sensors or their distance off the grid, or the size of the grid, whatever is smaller, seems plausible and leads to the same value of order 1 mm. For the initial vortex line density of order $10^8\,\mathrm{m}^{-2}$ (see Figure 19) thus the contribution of the evaporative decay mechanism ought to be small. Nevertheless, Nemirovskii[120] attempted to apply it to the Lancaster experiments of Bradley *et al.*[75] Although the simulated decay curves (see Figure 7 of Ref. 120) look similar to the experimental data shown in Figure 19, they lack the pronounced feature that all of the experimental decay data curves subsequently merge at the third universal classical regime of the form $L(t) \propto t^{-3/2}$. This seems to us a strong argument that our described above approach based on the decay of homogeneous and isotropic turbulence is justified. Nevertheless, the evaporative decay mechanism is interesting in its own right and is subject of current numerical research.

Let us speculate here that inhomogeneous classical turbulence generated in a viscous fluid by an oscillating grid decays both in time and diffuses away from the grid in a similar fashion as QT. In classical case it was indeed found and discussed in Ref. 8 that when the grid is stopped the spacial expansion affects the temporal decay of turbulent energy measured some distance from the grid only marginally, as the temporal decay was found to be in agreement with the prediction of crossover of power laws for decaying energy assuming homogeneous and isotropic turbulence.

IX. DISCUSSION OF THEORETICAL ASPECTS OF QT IN STATIONARY NORMAL FLUID

Let us discuss the Helsinki experimental results, already mentioned, obtained using the NMR technique in ^{3}He-B. In conventional liquids the vorticity $\boldsymbol{\omega} = curl\boldsymbol{v}$ obeys the Navier-Stokes equation, which we write here in the form,

$$\frac{\partial \boldsymbol{\omega}}{\partial t} = \nabla \times [\mathbf{v} \times \boldsymbol{\Omega}] + \nu\nabla^2\boldsymbol{\omega}. \tag{41}$$

The interplay of the two terms on the RHS, the inertial first term and the viscous second term, governs the transition to turbulence. It is determined by the external conditions through the Reynolds number, $Re = RU/\nu$, formed by the characteristic size R of the system, the flow velocity U, and the kinematic viscosity ν. For $Re \gg 1$, the effect of the inertial term dominates, and the laminar flow becomes increasingly unstable and turbulent. If vorticity is released into a metastable laminar state, a sudden transition to a chaotic flow of eddies occurs.

The vorticity of the superfluid component in ^{3}He-B is quantized in terms of the circulation quantum $\kappa = 2\pi\hbar/M$ where $M = 2m_3$ is the mass of a superfluid particle—a Cooper pair consisting of two ^{3}He atoms. The flow of the superfluid component can be characterized by the "superfluid Reynolds number" $Re_s = RU/\kappa$. The Feynman criterion $Re_s \sim 1$ gives the velocity at which it becomes energetically favorable to form a quantized vortex, but we already stated that a vortex is not always created upon exceeding this criterion. If a large nucleation barrier exists, the superfluid could remain vortex-free until much higher values of Re_s is reached. Quantized vortices can then be injected, either by some extrinsic means or by increasing the velocity so that the nucleation barrier is overcome and spontaneous vortex formation may occur.

In addition to the superflow, there is the normal component which is at rest in the container frame, $\boldsymbol{v}_n = 0$. Interactions between the superfluid vorticity and the normal component give rise to a mutual friction force on a unit volume of the superfluid,

$$\boldsymbol{f}_{mf} = -\alpha'\rho_s[\boldsymbol{v}_s \times \boldsymbol{\omega}_s] + \alpha\rho_s[\hat{\boldsymbol{\omega}}_s \times [\boldsymbol{\omega}_s \times \boldsymbol{v}_s]], \tag{42}$$

which is described by the dimensionless temperature-dependent parameters α and α', experimentally measured in ^{3}He-B by Bevan *et al.*[121] They correspond to the usual mutual friction

parameters if we are dealing with one vortex or locally polarized vorticity, or they may be renormalized in the general case. Here $\boldsymbol{v}_s$ and $\boldsymbol{\omega}_s = \nabla \times \boldsymbol{v}_s$ are the superfluid velocity and vorticity, and $\hat{\boldsymbol{\omega}}_s$ is the unit vector in the direction of $\boldsymbol{\omega}_s$. Inserting the mutual-friction force into the Euler equation after coarse-graining, Sonin obtains[122] the hydrodynamic equation for $Re_s \gg 1$,

$$\frac{\partial \boldsymbol{\omega}_s}{\partial t} = (1-\alpha')\nabla \times [\boldsymbol{v}_s \times \boldsymbol{\omega}_s] + \alpha \nabla \times [\hat{\boldsymbol{\omega}}_s \times (\boldsymbol{\omega}_s \times \boldsymbol{v}_s)]. \tag{43}$$

The energy dissipation is determined by the mutual friction damping α, while the reactive mutual-friction α' renormalizes the first term, the inertial term from Eq. (41). As in classical fluids, the inertial term drives the instability and is responsible for the energy transfer to smaller length scales, whereas the dissipative term acts to stabilize laminar flow. The fundamental difference from conventional hydrodynamics is that the relative importance of these two competing terms is determined by an intrinsic parameter of the superfluid, $q = \alpha/(1-\alpha')$, in contrast to classical liquids where it is governed via the Reynolds number by the extrinsic quantities R and U.

In the case of a single vortex line, as shown by Barenghi, Donnelly, and Vinen,[123] the parameter q marks the crossover from the regime where Kelvin waves can propagate along a vortex ($q < 1$) to where they are overdamped ($q > 1$). As explained by Kopnin,[124] in Fermi superfluids and superconductors with finite energy gap one has $q \approx (\omega_0 \tau)^{-1}$, where ω_0 is the spacing between the bound states of quasiparticles in the vortex core and τ^{-1} is their lifetime broadening, owing to scattering from the normal component. Based on measurements of α and α' in ^{3}He-B by Bevan *et al.*,[121] q approaches infinity at T_c and drops roughly exponentially to zero, when cooled down to $T \to 0$. In classical fluids this would correspond to scanning the Reynolds number from 0 to ∞.

The Helsinki data clearly show that the transition is surprisingly sharp between regular "high-temperature" processes (marked with open symbols in the phase diagram in Figure 23) and turbulent low temperature processes (filled symbols) observed at 0.60 T_c, with $N_f \sim 1$ above and $N_f \approx 10^3$ below the transition. The main conclusion is that the transition occurs as a function of temperature [or $q = q(T) = \alpha/(1-\alpha')$], with little or no dependence on the maximum superflow velocity $U = \Omega R$, in striking contrast to classical liquids.

A. Energy spectrum of quantum turbulence in a stationary normal fluid

We now consider possible shape of the energy spectrum of quantum turbulence in a stationary normal fluid. If quantized vortices are present, the superfluid velocity field is coupled to a stationary normal fluid by the mutual friction force, acting at all length scales. It has been shown by Vinen[125] that the superfluid eddies of all sizes would decay exponentially, with a characteristic decay time τ_{mf}. To appreciate the role of mutual friction in turbulent flow, τ_{mf} has to be compared with the eddy turnover time, τ_{to}, at any particular length scale. If $\tau_{mf} < \tau_{to}$, superfluid eddies cannot exist. Because the turnover time increases with the size of the eddy, Vinnen's analysis shows that eddies larger than the maximum size of the order,

$$R_{\max} \approx \left[\epsilon/(\alpha\kappa L)^3\right]^{1/2} \tag{44}$$

cannot exist. This is contrary to classical turbulence, where large eddies decay very little (the so-called permanence of large eddies) and their size is limited only by the boundaries of the container.

In further analysis we shall be interested only in scales that are large in comparison with the mean intervortex distance, in which case Eq. (43) can be written in a form similar to the Navier-Stokes equation,

$$\frac{\partial \mathbf{v}_s}{\partial t} + \nabla \mu = \mathbf{v}_s \times \boldsymbol{\omega}_s + q\hat{\boldsymbol{\omega}}_s \times (\boldsymbol{\Omega}_s \times \boldsymbol{v}_s), \tag{45}$$

where μ is the chemical potential. We recall that $\boldsymbol{\omega}_s$ denotes here the coarse-grained superfluid vorticity and the role of the effective Reynolds number is played by the parameter $Re_{\text{eff}} = q^{-1} = (1-\alpha')/\alpha$

which, via the mutual friction parameters α and α', depends on the temperature but not on the geometry.

L'vov, Nazarenko, and Volovik[126] and, independently, Vinen[125] analyzed this equation and showed that owing to the action of mutual friction, there is strong damping of large eddies, with the result that at low wave numbers the energy spectrum rolls off more rapidly, approaching k^{-3}. Beyond a certain critical value k_{cr}, however, the superfluid energy spectrum gradually recovers its usual Kolmogorov form, characterized by the $-5/3$ roll-off exponent.

B. Decaying counterflow turbulence in He II

We have already discussed the Prague second sound data on decaying counterflow turbulence and argued that they can usefully be divided into three stages. The last stage, where the turbulence decay follows Eq. (38), provided the first experimental evidence of dependence on the size of the channel.

Let us now turn attention to the early to middle stages of the decay, which are characterized by a considerably slower decay rate. What is puzzling is that a net *decrease* of the second sound amplitude $a(t)$ was observed at some parameters, as shown in Figure 27. The vortex line density $L(t)$ is usually determined from the measured second sound amplitude $a(t)$ assuming the vortex tangle to be homogeneous and isotropic. If it is polarized and the degree of polarization is not known, the second sound amplitude alone does not provide enough information to calculate the total vortex line density. This is why we plot in Figure 27 the quantity $a_0/a(t) - 1$, which refers directly to the transverse attenuation of second sound, not the total vortex line density, which is not known.

Gordeev *et al.*[47] speculated that the increase in time of the quantity $a_0/a(t) - 1$ can be explained by the fact that the vortex tangle in the steady-state counterflow turbulence is highly polarized by the applied counterflow; therefore, when the heater is switched off, the orientation of

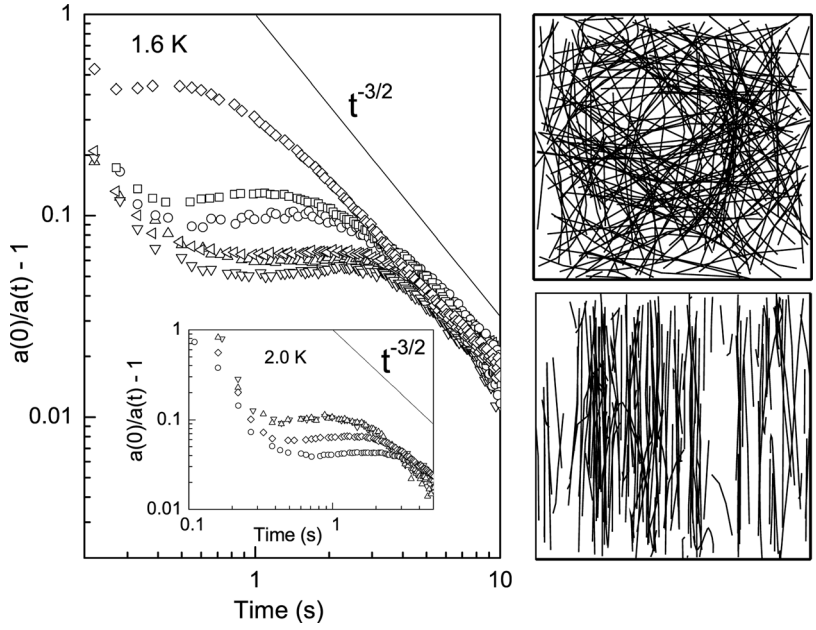

FIG. 27. Left: Log-log plot of the quantity $(a_0/a(t) - 1)$, where a_0 and $a(t)$ denote the initial and decaying second sound amplitude, versus time measured at $T = 1.6$ K. Under the assumption that the tangle is homogeneous and isotropic, this quantity would be proportional to the vortex line density L. For given experimental conditions, the level $a_0/a(t) - 1 = 0.1$ would correspond to the vortex line density $L \approx 10^5$ cm^{-2}. The different decay curves correspond to different initial levels of steady-state counterflow turbulence generated at powers 0.5 W ($\diamond$), 0.23 W (squares), 0.18 W ($\bigcirc$) and 0.14 W (various triangles), respectively. Three individual decay curves are shown to appreciate the level of reproducibility for the lowest applied power. The inset shows analogous data measured at $T = 2.0$ K; applied powers: 0.52 W (various triangles), 0.41 W ($\diamond$), and 0.32 W ($\bigcirc$). Right: Perpendicular and parallel projections of the initial vortex tangle resulting from the computer simulations clearly show that the vortex tangle is strongly polarized.

the vortex lines becomes more randomized. Indeed, if the tangle is fully polarized and all vortices are on planes perpendicular to the direction of the counterflow, since $\langle \sin^2 \rangle = 1/2$ averaged over the unit disk, the sensors detect $L/2$. If the tangle is isotropic, since $\langle \sin^2 \rangle = 2/3$ averaged over the unit sphere, the second sound sensors detect $2L/3$, yielding a factor of 4/3 higher.

Numerical simulations based on vortex filament method by Barenghi, Gordeev, and Skrbek[62] (see Figure 27) show that the vortex tangle induced by the counterflow is indeed polarized by the normal fluid along the channel. When the heater is switched off, this polarizing effect gradually ceases, and vortex reconnections play a more important role. Vortex loops, which were flattened in the plane across the channel in the steady-state, start turning around randomly when reconnecting. Hence the apparent vortex length which is "visible" by the second sound can increase according to the sine-squared law.

In the third stage of the decay of counterflow turbulence ($t > t_{sat}$), the vorticity acquires a universal classical $t^{-3/2}$ power law. The accepted physical picture of decaying grid generated He II turbulence assumes an existence of a range of normal and superfluid eddies (constituted of bundles of quantized vortex lines) coupled by the action of the mutual friction force. In practice, it is sufficient that a disordered system of vortex lines has enough polarization in the direction of the normal fluid vorticity so that effectively, in a coarse-grained sense, coupled normal fluid and superfluid eddies are formed. Therefore the most plausible interpretation of the experimental results is that, during the third stage of the decay (for $t > t_{\rm sat}$), we expect superfluid eddies ranging all the way up to the size of the channel. But if there are large superfluid eddies, these will interact via mutual friction with the normal fluid. Therefore the normal fluid is most likely driven into a turbulent state too, so that, in this stage of decay, the counterflow turbulence should indeed be similar in character to the decaying grid generated turbulence.

On the other hand, the properties of steady-state counterflow turbulence are well described by Vinen's equation, based on the assumption that the vortex tangle is random. Therefore, there are most likely no large superfluid (or normal) eddies. This might be understood as a consequence of a large mean counterflow velocity that (in the spanwise direction) tears apart the large normal and superfluid eddies, on a faster time scale than their turnover time.

Assuming that the physical picture outlined here of the structure of the vortex tangle in the first and third stages is correct, we are left to assume that the gradually larger and larger superfluid eddies grow during the second stage, until their size becomes saturated by the channel dimension. In fact, in steady-state we deal with almost two-dimensional turbulence, and the growth of eddies might be stimulated by the inverse energy cascade. As they grow, they must in turn generate normal eddies of large size too (due to the action of the mutual friction force—since the mean counterflow does not exist any more to tear them apart) so that, at the beginning of the third stage, the decaying counterflow and grid generated He II turbulence appear essentially the same and display the same decay.

C. A simple model for effective kinematic viscosity of turbulent He II

As far as we know, the first serious semi-quantitative phenomenological attempt to explain the observed temperature dependence of $\nu_{\rm eff}(T)$ in He II in frame of the two-fluid model is that by Vinen and Niemela in their comprehensive review on quantum turbulence.[3]

We will now present an alternative very simple model for effective kinematic viscosity in highly turbulent He II,[127] where the normal and superfluid velocity fields are coupled by the mutual friction force. At low k these are locked together, but as k increases toward k_Q, they gradually become decoupled due to combined action of the normal fluid viscosity and quantum effects in the superflow.

Let us assume, for order of magnitude estimates, that this uncoupling takes place not gradually, but at some characteristic k_d, so that for $k < k_d$, the normal and superfluid flows are fully coupled. Let us now consider a frame of reference of a particular normal fluid eddy of the size k_d and neglect possible motion of the normal fluid at higher k (i.e., we assume that for $k > k_d$ the normal fluid is at rest) and assume that, for $k > k_d$, there are enough quantized vortices, arranged in the flow in such a way that the coarse-grained hydrodynamic equation (45) holds. We remind the reader that the role of the effective Reynolds number is played by the parameter

$Re_{\rm eff} = q^{-1} = (1-\alpha')/\alpha$, which depends on the temperature but not on the geometry. As was first emphasized by Finne *et al.*,[68] Eq. (45) has very remarkable properties which make it distinct from the ordinary Navier-Stokes equation which can be written in a similar form,

$$\frac{\partial \boldsymbol{v}}{\partial t} + \nabla \mu = \boldsymbol{v} \times \boldsymbol{\omega} + \nu \nabla^2 \boldsymbol{v}. \tag{46}$$

Let us compare the dissipative terms on the RHS of Eqs. (45) and (46). Taking into account that $\boldsymbol{\omega} \simeq \kappa L \approx \kappa/\ell^2$, where ℓ is the characteristic intervortex distance, we estimate the superfluid dissipation term as $q\kappa \boldsymbol{v}/\ell^2$. By analogy with $\nabla^2 \mathbf{v} \approx \mathrm{v}/\ell^2$ we see that by an order of magnitude the effective kinematic viscosity must be given by $\nu_{\rm eff} \approx \kappa q$. We plot this quantity together with experimental data $\nu_{\rm eff}(T)$ in Figure 26. The qualitative agreement with the experimental data in He II suggests that it captures the underlying physics, at least approximately, and emphasizes the role of Eq. (45) in superfluid hydrodynamics. The model prediction is in good agreement with more sophisticated calculations by Roche, Barenghi, and Leveque,[101] displaying similar temperature dependence.

This very simple model cannot, of course, be used outside the region where its assumptions are valid, the most crucial ones being that the hydrodynamic description of superfluid is still valid beyond k_d (which ceases to be valid close to the λ-point) and that the dissipation in the superfluid occurs entirely via mutual friction (which ceases to be valid at very low temperature when dissipation by emission of phonons via Kelvin wave cascade dominates).

X. CONCLUSIONS

This review is essentially a summary of what we know about QT primarily from the experimental point of view. Our focus has been the hydrodynamic description of the most common superfluids, He II and ^{3}He-B. It is clear that the field of QT, which for some time had remained dormant, has sprung into great revival. The main point is that quantized vortices are the macroscopic manifestation of quantum phenomena, but that, for a number of considerations, further details of underlying quantum mechanics can be safely ignored. The extraordinary finding is the degree to which the usual hydrodynamic concepts can be used to describe various observations of developed QT in counterflow as well as co-flowing turbulent systems. Our arguments have been as quantitative as possible but are still primarily at the level of scaling. We have not paid too much attention to the theory or computational studies even though we have invoked them at various places. We have not paid particular attention, either, to various transitional studies in superfluids, on which a substantial body of literature exists (see, e.g., Ref. 3, 4 and references therein LSWFV and references therein).

QT is an interesting and challenging subject in its own right. It is our expectation that many new and interesting studies of QT will emerge. Such studies will enhance our understanding of not only the quantum systems but also classical systems. We hope that this short review is helpful to invite readers—members of the classical fluid dynamics community—to join our intriguing research in the field of quantum turbulence.

ACKNOWLEDGMENTS

The research of L.S. is supported by GAČR 202/08/0276 of the Czech Republic.

[1]The term Quantum Turbulence was introduced into the literature by R. J. Donnelly in a symposium dedicated to the memory of G. I. Taylor, see R. J. Donnelly and C. E. Swanson, "Quantum turbulence," J. Fluid Mech. **173**, 387 (1986).
[2]R. P. Feynman, "Application of quantum mechanics to liquid helium," in *Progress in Low Temperature Physics*, edited by C. J. Gorter (North Holland, Amsterdam, 1955), Vol. 1.
[3]W. F. Vinen and J. J. Niemela, "Quantum turbulence," J. Low Temp. Phys. **128**, 167 (2002).
[4]L. Skrbek, "Turbulence in cryogenic helium," Physica C **404**, 354 (2004).
[5]W. F. Vinen, "Mutual friction in a heat current in liquid helium II, I. Experiments on steady heat currents," Proc. R. Soc. A **240** 114 (1957); "II. Experiments on transient effects," *ibid.* **240**, 128 (1957); "III. Theory of the mutual friction," *ibid.* **242**, 493 (1957); "IV. Critical heat currents in wide channels," *ibid.* **243**, 400 (1958).
[6]J. Maurer and P. Tabeling, "Local investigation of superfluid turbulence," Europhys. Lett. **43**, 29 (1998).
[7]M. R. Smith, R. J. Donnelly, N. Goldenfeld, and W. F. Vinen, "Decay of vorticity in homogeneous turbulence," Phys. Rev. Lett. **71**, 2583 (1993).
[8]S. R. Stalp, L. Skrbek, and R. J. Donnelly, "Decay of grid turbulence in a finite channel," Phys. Rev. Lett. **82**, 4831 (1999).
[9]W. F. Vinen, "Classical character of turbulence in a quantum liquid," Phys. Rev. B **61**, 1410 (2000).

[10]R. J. Donnelly and C. F. Barenghi, "The observed properties of liquid helium at the saturated vapor pressure," J. Phys. Chem. Ref. Data **27**, 1217 (1998).
[11]J. J. Niemela, L. Skrbek, K. R. Sreenivasan, and R. J. Donnelly, "Turbulent convection at very high Rayleigh numbers," Nature (London) **404**, 837 (2000).
[12]R. J. Donnelly and K. R. Sreenivasan, *Flow at Ultra-High Reynolds and Rayleigh Numbers* (Springer, New York, 1998).
[13]L. Skrbek, J. J. Niemela, and R. J. Donnelly, "Turbulent flows at cryogenic temperatures: A new frontier," J. Phys.: Condens. Matter **11**, 7761 (1999).
[14]J. J. Niemela and K. R. Sreenivasan, "The use of cryogenic helium for classical turbulence: Promises and hurdles," J. Low Temp. Phys. **143**, 163 (2006).
[15]D. R. Tilley and J. Tilley, *Superfluidity and Superconductivity* (Adam Hilger, 1986).
[16]L. D. Landau and E. M. Lifshitz, *Hydrodynamics*, 2nd ed. (Pergamon Press, New York, 1987).
[17]E. L. Andronikashvili, "A direct observation of two kinds of motion in helium II," J. Phys. (Moscow) **10**, 201 (1946).
[18]L. Onsager, in discussion on paper by C. J. Gorter, Nuovo Cimento **6** (Suppl. 2), 249 (1949); "Introductory talk," in Proceedings of the International Conference of Theoretical Physics (Kyoto and Tokyo, 1953), p. 877; for further details see Chap. II of Ref. 19.
[19]R. J. Donnelly, *Quantized Vortices in Helium II* (Cambridge University Press, Cambridge, 1991).
[20]D. V. Osborne, "The rotation of liquid helium-II," Proc. Phys. Soc. A **63**, 909 (1950).
[21]E. J. Yarmchuk, M. V. G. Gordon, and R. E. Packard, "Observation of stationary vortex arrays in rotating superfluid helium," Phys. Rev. Lett. **43**, 214 (1979).
[22]G. P. Bewley, D. P. Lathrop, and K. R. Sreenivasan, "Superfluid helium—Visualization of quantized vortices," Nature (London) **441**, 588 (2006).
[23]J. T. Tough, "Superfluid turbulence," in *Progress in Low Temperature Physics* (North-Holland Publ. Co., 1982), Vol. VIII.
[24]L. Skrbek and W. F. Vinen, "The use of vibrating structures in the study of quantum turbulence," in *Progress in Low Temperature Physics* edited by M. Tsubota and W. P. Halperin (Elsevier, Amsterdam, 2009), Vol. XVI, Chap. 4.
[25]This term was written by Gorter and Mellink (see Ref. 31) in the form $A\rho_s\rho_n(v_s - v_n)^3$ already in 1949, before quantized vortices were introduced by Onsager (see Ref. 18) and Feynman (see Ref. 2).
[26]H. E. Hall and W. F. Vinen, "The rotation of liquid helium-II. 1. Experiments on the propagation of 2nd sound in uniformly rotating helium–II," Proc. R. Soc. London Ser. A **238**, 204 (1956);"The rotation of liquid helium-II. 2. The theory of mutual friction in in uniformly rotating helium–II," **238**, 215 (1956).
[27]K. W. Schwarz, "Turbulence in superfluid-helium—steady homogeneous counterflow," Phys. Rev. B **18**, 245 (1978); "3-dimensional vortex dynamics in superfluid He-4—line-line and line–boundary interactions," *ibid.* **31**, 5782 (1985); "Critical velocity for a self-sustaining vortex tangle in superfluid helium," Phys. Rev. Lett. **50**, 364 (1983).
[28]K. W. Schwarz, "Three-dimensional vortex dynamics in superfluid He-4—homogeneous superfluid turbulence," Phys. Rev. B **38**, 2398 (1988).
[29]J. J. Thomson, "Vibrations of a columnar vortex," Philos. Mag. **10**, 155 (1880).
[30]L. Skrbek, A. V. Gordeev, and F. Soukup, "Decay of counterflow He II turbulence in a finite channel: Possibility of missing links between classical and quantum turbulence," Phys. Rev. E **67**, 047302 (2003).
[31]C. J. Gorter and J. H. Mellink, "On irreversible processes in liquid helium–II," Physica **15**, 285 (1949).
[32]C. E. Swanson and R. J. Donnelly, "Vortex dynamics and scaling in turbulent counterflowing helium II," J. Low Temp. Phys. **61**, 363 (1985).
[33]J. F. Allen and J. Reekie, "Momentum transfer and heat flow in liquid helium II," Proc. Cambridge Philos. Soc. **35**, 114 (1939).
[34]D. D. Awschalom, F. P. Milliken, and K. W. Schwarz, "Properties of superfluid turbulence in a large channel," Phys. Rev. Lett. **53**, 1372 (1984).
[35]D. F. Brewer and D. O. Edwards, "Heat conduction by liquid helium in capillary tubes. 2. Measurements of the pressure gradient," Philos. Mag. **6**, 1173 (1961).
[36]C. E. Chase, "Thermal conduction in liquid He II. 1. Temperature dependence," Phys. Rev. **127**, 361 (1962); "Thermal conduction in liquid He II. 2. Effects of channel geometry," *ibid.* **131**, 1898 (1963).
[37]H. Adachi, S. Fyjiyama, and M. Tsubota, "Steady-state counterflow quantum turbulence: Simulation of vortex filaments using the full Biot-Savart law," Phys. Rev. B **81**, 104511 (2010).
[38]D. J. Melotte and C. F. Barenghi, "Transition to normal fluid turbulence in helium II," Phys. Rev. Lett. **80**, 4181 (1998).
[39]S. W. van Sciver, S. Fuzier, and T. Xu, "Particle image velocimetry studies of counterflowing heat transport in superfluid helium II," J. Low Temp. Phys. **148**, 225 (2007).
[40]M. S. Paoletti, M. E. Fisher, K. R. Sreenivasan, and D. P. Lathrop, "Velocity statistics distinguish quantum turbulence from classical turbulence," Phys. Rev. Lett. **101**, 154501 (2008).
[41]Y. A. Sergeev and C. F. Barenghi, "Particles-vortices interactions and flow visualization in He-4," J. Low Temp. Phys. **157**, 429 (2009).
[42]A. C. White, C. F. Barenghi, N. P. Proukakis, A. J. Youd, and D. H. Wacks, "Nonclassical velocity statistics in a turbulent atomic Bose-Einstein Condensate," Phys. Rev. Lett. **104**, 075301 (2010).
[43]W. Guo, S. B. Cahn, J. A. Nikkel, W. F. Vinen, and D. N. McKinsey, "Visualization study of counterflow in superfluid ^{4}He using metastable helium molecules," Phys. Rev. Lett. **105**, 045301 (2010).
[44]W. Guo, J. D. Wright, S. B. Cahn, J. A. Nikkel, and D. N. McKinsey, "Metastable helium molecules as tracers in superfluid He-4," Phys. Rev. Lett. **102**, 235301 (2009).
[45]C. F. Barenghi, C. E. Swanson, and R. J. Donnelly, "Induced vorticity fluctuations in counterflowing He II," Phys. Rev. Lett. **48**, 1187 (1982).
[46]K. W. Schwarz, and J. R. Rozen, "Anomalous decay of turbulence in superfluid He – 4," Phys. Rev. Lett. **66**, 1898 (1991); "Transient-behavior of superfluid turbulence in a large channel," Phys. Rev. B **44**, 7563 (1991).
[47]A. V. Gordeev, T. V. Chagovets, F. Soukup, and L. Skrbek, "Decaying counterflow turbulence in He II," J. Low Temp. Phys. **138**, 549 (2005).
[48]K. R. Sreenivasan, "On the universality of the Kolmogorov constant," Phys. Fluids **7**, 27788 (1995).
[49]J. Salort, C. Baudet, B. Castaing, B. Chabaud, F. Daviaud, T. Didelot, P. Diribarne, B. Dubrulle, Y. Gagne, F. Gauthier, A. Girard, B. Hebral, B. Rousset, P. Thibault, and P. E. Roche, "Turbulent velocity spectra in superfluid flows," Phys. Fluids **22**, 125102 (2010).

[50]J. C. Bennett and S. Corrsin, "Small Reynolds number nearly isotropic turbulence in a straight duct and a contraction," Phys. Fluids **21**, 2129 (1978).
[51]G. Comte-Bellot and S. Corrsin, "The use of a contraction to improve the isotropy of grid-generated turbulence," J. Fluid Mech. **25**, 657 (1966).
[52]A. L. Kistler and T. Vrebalovich, "Grid turbulence at large Reynold numbers," J. Fluid Mech. **26**, 37 (1966).
[53]I. P. D. De Silva and H. J. S. Fernando, "Oscillating grids as a source of nearly isotropic turbulence," Phys. Fluids **6**, 2455 (1994).
[54]E. van Doorn, C. M. White, and K. R. Sreenivasan, "The decay of grid turbulence in polymer and sufactant solutions," Phys. Fluids **11**, 2387 (1999).
[55]P. G. Saffman, "Note on decay of homogeneous turbulence," J. Fluid Mech. **27**, 581 (1967); Phys. Fluids **10**, 1349 (1967).
[56]L. Skrbek and S. R. Stalp, "On the decay of homogeneous isotropic turbulence," Phys. Fluids **12**, 1997 (2000).
[57]G. L. Eyink and D. J. Thomson, "Free decay of turbulence and breakdown of self-similarity," Phys. Fluids **12**, 477 (2000).
[58]L. Skrbek, J. J. Niemela, and R. J. Donnelly, "Four regimes of decaying grid turbulence in a finite channel," Phys. Rev. Lett. **85**, 2973 (2000).
[59]S. R. Stalp, J. J. Niemela, W. F. Vinen, and R. J. Donnelly, "Dissipation of grid turbulence in helium II," Phys. Fluids **14**, 1377 (2002).
[60]J. J. Niemela, K. R. Sreenivasan, and R. J. Donnelly, "Grid generated turbulence in helium II," J. Low Temp. Phys. **138**, 537 (2005).
[61]S. R. Stalp, "Decay of grid turbulence in superfluid helium," Ph.D. thesis (University of Oregon, Eugene, OR, 1998).
[62]C. F. Barenghi, A. V. Gordeev, and L. Skrbek, "Depolarization of decaying counterflow turbulence in He II," Phys. Rev. E **74**, 026309 (2006).
[63]H. A. Snyder and Z. Putney, "Angular dependence of mutual friction in rotating helium 2," Phys. Rev. **150**, 110 (1966).
[64]P. Mathieu, B. Placais, and Y. Simon, "Spatial-distribution of vortices and anisotropy of mutual friction in rotating He II," Phys. Rev. B **29**, 2489 (1984).
[65]F. P. Milliken, K. W. Schwarz, and C. W. Smith, "Free decay of superfluid turbulence," Phys. Rev. Lett. **48**, 1204 (1982).
[66]S. I. Davis, P. C. Hendry, and P. V. E. McClintock, "Decay of quantized vorticity in superfluid He-4 at mK temperatures," Physica B **280**, 43 (2000).
[67]G. G. Ihas, G. Labbe, S. C. Liu, and K. Thomson, "Preliminary measurements on grid turbulence in liquid ^{4}He," J. Low Temp. Phys. **150**, 384 (2007).
[68]A. P. Finne, T. Araki, R. Blaauwgeers, V. B. Eltsov, N. B. Kopnin, M. Krusius, L. Skrbek, M. Tsubota, and G. E. Volovik, "Observation of an intrinsic velocity-independent criterion for superfluid turbulence," Nature (London) **424**, 1022 (2003).
[69]V. B. Eltsov, R. de Graaf, R. Hanninen, M. Krusisus, R. E. Solntsev, V. S. L'vov, A. I. Golov, and P. M. Walmsley, "Turbulent dynamics in rotating helium superfluids," in *Progress in Low Temperature Physics*, edited by M. Tsubota and W. P. Halperin (Elsevier, Amsterdam, 2009), Vol. XVI, Chap. 2.
[70]D. I. Bradley, D. O. Clubb, S. N. Fisher, A. M. Guenault, C. J. Matthews, and G. R. Pickett, "Vortex generation in superfluid He-3 by a vibrating grid," J. Low Temp. Phys. **134**, 381 (2004).
[71]G. R. Pickett and S. N., Fisher, "Superfluid He-3 in the zero-temperature limit," Physica B **329**, 75 (2003).
[72]S. N. Fisher and G. R. Pickett, "Quantum turbulence in superfluid ^{3}He at very low temperatures," in *Progress in Low Temperature Physics*, edited by M. Tsubota and W. P. Halperin (Elsevier, Amsterdam, 2009), Vol. XVI, Chap. 3.
[73]D. I. Bradley, D. O. Clubb, S. N. Fisher, A. M. Guenault, R. P. Haley, C. J. Matthews, G. R. Pickett, V. Tsepelin, and K. Zaki, "Emission of discrete vortex rings by a vibrating grid is superfluid He-3-B: A precursor to quantum turbulence," Phys. Rev. Lett. **95**, 305302 (2005).
[74]S. Fujiyama, A. Mitani, M. Tsubota, D. I. Bradley, S. N. Fisher, A. M. Gunault, R. P. Haley, G. R. Pickett, and V. Tsepelin, "Generation, evolution, and decay of pure quantum turbulence: A full Biot-Savart simulation," Phys. Rev. B **81**, 026309R (2010).
[75]D. I. Bradley, D. O. Clubb, S. N. Fisher, A. M. Guenault, R. P. Haley, C. J. Matthews, G. R. Pickett, V. Tsepelin, and K. Zaki, "Decay of pure quantum turbulence in superfluid He-3-B," Phys. Rev. Lett. **96**, 035301 (2006).
[76]D. I. Bradley, S. N. Fisher, A. M. Guenault, R. P. Haley, S. O'Sullivan, G. R. Pickett, and V. Tsepelin, "Fluctuations and correlations of pure quantum turbulence in superfluid He-3-B," Phys. Rev. Lett. **101**, 065302 (2008).
[77]P. E. Roche, P. Diribarne, T. Didelot, O. Francais, L. Rousseau, and H. Willaime, "Vortex density spectrum of quantum turbulence," Europhys. Lett. **77**, 66002 (2007).
[78]P. E. Roche and C. F. Barenghi, "Vortex spectrum in superfluid turbulence: Interpretation of a recent experiment," Europhys. Lett. **81**, 36002 (2008).
[79]D. I. Bradley, S. N. Fisher, A. M. Guenault, R. P. Haley, G. R. Pickett, D. Potts, and V. Tsepelin, "Direct measurement of the energy dissipated by quantum turbulence," Nat. Phys. **7**, 473 (2011).
[80]P. M. Walmsley, A. I. Golov, H. E. Hall, A. A. Levchenko, and W. F. Vinen, "Dissipation of quantum turbulence in the zero temperature limit," Phys. Rev. Lett. **99**, 265302 (2007).
[81]P. M. Walmsley and A. I. Golov, "Quantum and quasiclassical types of superfluid turbulence," Phys. Rev. Lett. **100**, 245301 (2008).
[82]P. M. Walmsley, A. I. Golov, H. E. Hall, W. F. Vinen, and A. A. Levchenko, "Decay of turbulence generated by spin-down to rest in superfluid He-4," J. Low Temp. Phys. **153**, 127 (2008).
[83]A. I. Golov, P. M. Walmsley, and P. A. Tompsett, "Charged tangles of quantized vortices in superfluid He-4," J. Low Temp. Phys. **161**, 509 (2010).
[84]R. Blaauwgeers, V. B. Eltsov, G. Eska, A. P. Finne, R. P. Haley, M. Krusius, J. J. Ruohio, L. Skrbek, and G. E. Volovik, "Shear flow and Kelvin-Helmholtz instability in superfluids," Phys. Rev. Lett. **89**, 155301 (2002).
[85]J. S. Korhonen, A. D. Gongadze, Z. Janu, Y. Kondo, M. Krusius, Y. M. Mukharsky, and E. V. Thuneberg, "Order parameter textures and boundary conditions in rotating vortex-free He-3-B," Phys. Rev. Lett. **65**, 1211 (1990).
[86]V. B. Eltsov, A. P. Finne, R. Hanninen, J. Kopu, M. Krusius, M. Tsubota, and E. V. Thuneberg, "Twisted vortex state," Phys. Rev. Lett. **96**, 215302 (2006).

[87]V. B. Eltsov, A. I. Golov, R. de Graaf, R. Hänninen, M. Krusius, V. S. Lvov, and R. E. Solntsev, "Quantum turbulence in a propagating superfluid vortex front," Phys. Rev. Lett. **99**, 265301 (2007).
[88]L. Skrbek, J. J. Niemela, and K. R. Sreenivasan, "Energy spectrum of grid-generated He II turbulence," Phys. Rev. E **64**, 067301 (2001).
[89]J. Koplik and H. Levine, "Vortex reconnection in superfluid-helium," Phys. Rev. Lett. **71**, 1375 (1993).
[90]M. Leadbeater, T. Winiecki, D. C. Samuels, C. F. Barenghi, and C. S. Adams, "Sound emission due to superfluid vortex reconnections," Phys. Rev. Lett. **86**, 1410 (2001).
[91]S. Ogawa, M. Tsubota, and Y. Hattori, "Study of reconnection and acoustic emission of quantized vortices in superfluid by the numerical analysis of the Gross-Pitaevskii equation," J. Phys. Soc. Jpn. **71**, 813 (2002).
[92]C. F. Barenghi, N. G. Parker, N. P. Proukakis, and C. S. Adams, "Decay of quantised vorticity by sound emission," J. Low Temp. Phys. **138**, 629 (2005).
[93]E. V. Kozik and B. V. Svistunov, "Kelvin-wave cascade and decay of superfluid turbulence," Phys. Rev. Lett. **92**, 035301 (2004); "Scale-separation scheme for simulating superfluid turbulence: Kelvin-wave cascade," *ibid.* **94**, 025301 (2005); "Vortex-phonon interaction," Phys. Rev. B **72**, 172505 (2005); "Kolmogorov and Kelvin-wave cascades of superfluid turbulence at $T = 0$: What lies between," *ibid.* **77**, 060502 (2008); "Scanning superfluid turbulence cascade by its low-temperature cutoff," Phys. Rev. Lett. **100**, 195302 (2008).
[94]V. S. Lvov, S. V. Nazarenko, and O. Rudenko, "Bottleneck crossover between classical and quantum superfluid turbulence," Phys. Rev. B **76**, 024520 (2007).
[95]T. Araki, M. Tsubota, and S. K. Nemirovskii, "Energy spectrum of superfluid turbulence with no normal-fluid component," Phys. Rev. Lett. **89**, 145301 (2002).
[96]C. Nore, M. Abid, and M. Brachet, "Kolmogorov turbulence in low-temperature superlows," Phys. Rev. Lett. **78**, 3296 (1997).
[97]M. Kobayashi and M. Tsubota, "Kolmogorov spectrum of superfluid turbulence: Numerical analysis of the Gross-Pitaevskii equation with a small-scale dissipation," Phys. Rev. Lett. **94**, 065302 (2005).
[98]V. S. L'vov, S. V. Nazarenko, and L. Skrbek, "Energy spectra of developed turbulence in helium superfluids," J. Low Temp. Phys. **145**, 125 (2006).
[99]J. Tchoufag and P. Sagaut, "Eddy damped quasinormal Markovian simulations of superfluid turbulence in helium II," Phys. Fluids **22**, 125103 (2010).
[100]D. Kivotides, "Coherent structure formation in turbulent thermal superfluids," Phys. Rev. Lett. **96**, 175301 (2006).
[101]P. E. Roche, C. F. Barenghi, and E. Leveque, "Quantum turbulence at finite temperature: The two-fluids cascade," Europhys. Lett. **87**, 54006 (2009).
[102]M. Lesieur, *Turbulence in Fluids*, 3rd ed. (Kluwer, Dordrecht, 1997).
[103]T. von Kármán and L. Horwath, "On the statistical theory of isotropic turbulence," Proc. R. Soc. London Ser. A **164**, 192 (1938).
[104]A. N. Kolmogorov, "On degeneration (decay) of isotropic turbulence in an incompressible viscous fluid," Dokl. Akad. Nauk SSSR **31**, 538 (1941).
[105]V. Yakhot, "Decay of three-dimensional turbulence at high Reynolds numbers," J. Fluid Mech. **505**, 87 (2004).
[106]L. G. Loitsianskii, "Some basic laws for isotropic turbulent flow," Trudy Tsentr. Aero.-Gidrodyn. Inst. **3**, 33 (1939).
[107]K. R. Sreenivasan, "On the scaling of the turbulence energy dissipation rate," Phys. Fluids **27**, 1048 (1984).
[108]C. Morize and F. Moisy, "Energy decay of rotating turbulence with confinement effects," Phys. Fluids **18**, 065107 (2006).
[109]V. Borue and S. A. Orszag, "Self-similar decay of three-dimensional homogeneous turbulence with hyperviscosity," Phys. Rev. E **5**, R856 (1995).
[110]L. Biferale, G. Bofetta, A. Celani, A. Lanotte, F. Toschi, and M. Vergassola, "The decay of homogeneous anisotropic turbulence," Phys. Fluids **15**, 2105 (2003).
[111]H. Touil, J. P. Bertoglio, and L. Shao, "The decay of turbulence in a bounded domain," J. Turbul. **3**, 049 (2002).
[112]D. A. Donzis, P. K. Yeung, and K. R. Sreenivasan, "Dissipation and enstrophy in isotropic turbulence: Resolution effects and scaling in direct numerical simulations," Phys. Fluids **20**, 045108 (2008).
[113]I. Proudman and W. H. Raid, "On the decay of a normally distributed and homogeneous turbulent velocity field," Philos. Trans. R. Soc. London A **247**, 163 (1954).
[114]T. Ishida, P. A. Davidson, and Y. Kaneda, "On the decay of isotropic turbulence," J. Fluid Mech. **564**, 455 (2006).
[115]T. V. Chagovets, A. V. Gordeev, and L. Skrbek, "Effective kinematic viscosity of turbulent He II," Phys. Rev. E **76**, 027301 (2007).
[116]T. V. Chagovets and L. Skrbek, "Steady and decaying flow of He II in channels with ends blocked by superleaks," Phys. Rev. Lett. **100**, 215302 (2008).
[117]T. V. Chagovets and L. Skrbek, "On flow of He II in channels with ends blocked by superleaks," J. Low Temp. Phys. **153**, 162 (2008).
[118]C. F. Barenghi and D. Samuels, "Evaporation of a packet of quantized vorticity," Phys. Rev. Lett. **89**, 155302 (2002).
[119]M. Tsubota, T. Araki, and W. F. Vinen, "Diffusion of an inhomogeneous vortex tangle," Physica B **329**, 224 (2003).
[120]S. K. Nemirovskii, "Diffusion of inhomogeneous vortex tangle and decay of superfluid turbulence," Phys. Rev. B **81**, 064512 (2010).
[121]T. D. C. Bevan, A. J. Manninen, J. B. Cook, H. Alles, J. R. Hook, and H. E. Hall, "Vortex mutual friction in superfluid He–3," J. Low Temp. Phys. **109**, 423 (1997).
[122]E. B. Sonin, "Vortex oscillations and hydrodynamics of rotating superfluids," Rev. Mod. Phys. **59**, 87 (1987).
[123]C. F. Barenghi, R. J. Donnelly, and W. F. Vinen, "Thermal excitations of waves on quantized vortices," Phys. Fluids **28**, 498 (1985).
[124]N. B. Kopnin, *Theory of Nonequilibrium Superconductivity* (Clarendon Press, Oxford, 2001).
[125]W. F. Vinen, "Theory of quantum grid turbulence in superfluid ^{3}He-B," Phys. Rev. B **71**, 024513 (2005).
[126]V. S. L'vov, S. V. Nazarenko, and G. E. Volovik, "Energy spectra of developed superfluid turbulence," JETP Lett. **80**, 479 (2004).
[127]L. Skrbek, "A simple phenomenological model for the effective kinematic viscosity of helium superfluids," J. Low Temp. Phys. **161**, 555 (2010).